

Article

Historical Pigments and Paint Layers: Raman Spectral Library with 852 nm Excitation Laser

Silvia Innocenti ^{1,2} , Diego Quintero Balbas ¹ , Monica Galeotti ³, Andrea Cagnini ³, Simone Porcinai ³ and Jana Striova ^{1,*} 

¹ National Research Council—National Institute of Optics (CNR-INO), Largo E. Fermi 6, 50125 Florence, FI, Italy; silvia.innocenti@ino.cnr.it (S.I.); diegoivan.quinterobalbas@ino.cnr.it or diegoivan.quinterobalbas@cnr.it (D.Q.B.)

² Department of Sciences of Antiquity, “La Sapienza” University of Rome, Piazzale Aldo Moro 5, 00186 Rome, RM, Italy

³ Opificio Delle Pietre Dure, Viale F. Strozzi, 1, 50129 Florence, FI, Italy; monica.galeotti@cultura.gov.it (M.G.); andrea.cagnini@beniculturali.it (A.C.); simone.porcinai@cultura.gov.it (S.P.)

* Correspondence: jana.striova@cnr.it

Abstract: Raman spectroscopy (RS), for its robust analytical capabilities under constant development, is a powerful method for the identification of various materials, in particular pigments in cultural heritage. Characterization of the artist’s palette is of fundamental importance for the correct formulation of restoration intervention as well as for preventive conservation of artworks. Here we examine the number and variability of research studies exploiting Bravo handheld Raman spectrophotometer relying on the excitation of Raman signal with temperature-shifted diode lasers emitting at 852 and 785 nm. To this end, we explore the spectral features of common historical pigments examined as powders and in the paint layer. We show that some materials may exhibit slightly different spectra as concerns especially the relative intensity of Raman lines with 852 nm laser excitation wavelength as compared to the standard 785 nm. The aim is to provide the research community with a reference spectral database that facilitates the identification of unknown pigments using the 852 nm excitation source.

Keywords: database; historical pigments; paint layers; Raman spectroscopy; 852 nm excitation laser



Citation: Innocenti, S.; Quintero Balbas, D.; Galeotti, M.; Cagnini, A.; Porcinai, S.; Striova, J. Historical Pigments and Paint Layers: Raman Spectral Library with 852 nm Excitation Laser. *Minerals* **2024**, *14*, 557. <https://doi.org/10.3390/min14060557>

Academic Editor: Lluís Casas

Received: 24 April 2024

Revised: 24 May 2024

Accepted: 27 May 2024

Published: 28 May 2024



Copyright: © 2024 by the authors. Licensee MDPI, Basel, Switzerland. This article is an open access article distributed under the terms and conditions of the Creative Commons Attribution (CC BY) license (<https://creativecommons.org/licenses/by/4.0/>).

1. Introduction

The identification of pigments in artworks may provide relevant information to date/detect forgeries, establish the artwork’s origin, or formulate suitable restoration and preventive conservation procedures. Raman spectroscopy is nowadays a well-established method in the field of heritage science for its capacity to identify non-destructively and non-invasively a large variety of art materials [1]. The development of increasingly efficient low-size and lightweight Raman micro-probes enables in situ measurements and investigation of the artwork without any movement, sampling, or damage [2]. A robust spectral database of reference substances might ease the interpretation and exploitation of Raman spectral information, recently also through automated processes. Numerous Raman spectral databases have been developed (Table 1) with the first online databases of Raman spectra libraries dating back to the 1990s. Among the most frequently exploited libraries, we can list those provided by University College London (UCL) [3], Infrared and Raman Users Group (IRUG) [4], INFRA-ART by the Romanian database of Raman spectroscopy [5], RRUFF™ by University of Arizona [6], Infrared and Raman Discussion Group (IRDG) [7], SOPRANO [8], and Cultural Heritage Science Open Source (CHSOS) [9]. The last two databases are particularly focused on pigments of historical and artistic interest. In addition to the digitally available spectral datasets, publications containing Raman spectra compendia on art-related materials are available in the literature [10]. Despite the

recent open-source policies that should provide findable, accessible, and reusable (FAIR) data, most of the spectral databases focused on cultural heritage materials display the Raman spectra only as images, therefore, limiting the usability of the information. A further limitation on the applicability of the databases is the fact that it is easier to obtain spectra informative enough when studying pure powder pigments; but when complex mixtures (i.e., paint layers containing a binder, pigment, and fillers) are analyzed, interference mainly arises from the organic substances employed as binders and/or varnishes. For this reason, it is fundamental to cross-check the applicability of the databases also in composite samples, for example, the SOPRANO and CHSOS databases.

Table 1. Overview of the main published (1997–2019) reference Raman spectral libraries of artistic materials, their accessibility, examined material, and excitation wavelength.

Libraries	Data Format	Analyzed Materials	Excitation Wavelength (nm)
ULC [3]	Online	Natural and synthetic pigments	514, 633
IRUG [11]	Online	Minerals, pigments, organic dyes, synthetic resins	532, 633, 785
Romanian Database of Raman Spectroscopy [12]	Online	Minerals	532
RRUFF [6]	Online	Minerals and pigments	532, 785
IRDG	Online	Pigments	1062
SOPRANO [13]	Online	Synthetic organic pigments (SOPs)	785
CHSOS—Pigments Checker [9]	Online	Pigments	532, 638, 785, 830, 1064
CAMEO Materials database (Museum of Fine Arts—Boston)	Online	Pigments and other art materials	514, 532, 632, 785
Vandenabeele et al. [14]	Published paper	Azo pigments	785
Burgio and Clark [10]	Published paper	Pigments, minerals, pigments media, and varnishes	514, 633, 647, 780, 1064
Bouchard and Smith [15]	Published paper	Minerals on corroded metals and colored glass	514, 632
Scherrer et al. [16]	Published paper	Synthetic organic pigments	514, 633, 785
Martina et al. [17]	Published paper	Silver corrosion products	532
Pozzi et al. [18]	Published paper	Watercolor’s dyes	488, 785
Coccatto et al. [19,20]	Published paper	Carbon-based black pigments and green minerals	532, 785
Marucci et al. [21]	Published paper	Medieval pigments	488, 532, 633, 785, 830
Culka and Jehlicka [22]	Published paper	Gemstones	785, 852
ColoRaman database [23]	No longer available online	Oil, tempera, and fresco paint pigments	531, 633, 780
E-Visart [24]	No longer available online	Pigments	785, 1062
Sessa et al. [25]	Published paper	Synthetic organic pigments (SOPs) in watercolor, tempera, and oil paints	532, 638, 785

As observed in Table 1, the libraries are commonly obtained with different excitation lines, because often the pigments’ response varies according to laser irradiation due to the Raman scattering cross-section and physical and optical properties. Generally, the selection of the excitation sources in the UV or NIR spectral regions may minimize the fluorescence interference. However, the Raman signal obtained with NIR lines is weaker than that obtained with lasers in the visible range because the Raman scattering strength is proportional to the fourth power of the excitation frequency [26]. In addition, excellent Raman enhancement can be obtained through the Resonance Raman effect, produced when the laser wavelength matches the absorption bands of the pigment. Moreover, the absorption of the laser radiation can lead to a reduction in the signal and induce interferences [1].

Photoluminescence from either the sample or the substrate may produce signals on the order of or sometimes greater than the Raman signal itself. These phenomena can have an impact on the final Raman spectra, depending on the employed laser wavelength, highlighting or hiding chemical information from the sample. As a consequence, the Raman spectrum of one pigment can appear different depending on whether the laser excitation is in resonance with an electronic transition or whether other photoluminescence bands appear. The literature reporting on the spectral pigments databases includes laser excitation sources, such as Ar⁺ (488 and 514 nm) or Kr⁺ (531 and 647 nm), He:Ne (633 nm), Nd:YAG (532 and 1064 nm), and diode laser (630 and 785 nm) [27].

The recently released handheld spectrophotometer by Bruker Optics, commercially named Bravo, employs two different excitation lasers (852 and 785 nm) to cover a spectral range initially comprised between 300 and 3200 cm⁻¹ [28]. After 2020, the instrument spectral range was extended to cover a wider range comprised between 170 and 3200 cm⁻¹, which was a significant improvement, particularly for the investigation of inorganic compounds. The sequentially shifted excitation technology (SSETM) and the PCA-based algorithm are exploited to provide the processed background-free and smoothed spectra. This processing procedure is particularly helpful in solving the common background collection produced by the short optical paths typical of portable instrumentation [29], as well as from the strong luminescence produced by cultural heritage organic materials. The application of Bravo Raman has increased considerably in the heritage science field as is evidenced by the recently published scientific literature (Figure 1). The trend of the employment of the instrumentation is exponential, with a decrease in 2020 corresponding to the COVID-19 pandemic. Bravo spectrophotometer proved powerful in addressing research problems pertinent to the identification of historical and modern pigments and lakes [30–53], minerals and gems [22,29,54], manuscripts [55,56], mosaics [2,57], and metal and metal corrosion products [58–60]. The present work aims to create a database using the 852 nm laser excitation wavelength for the most commonly employed art pigments, which can be regarded as the precursor of a larger open-source database of artistic colorants that is expected to be available online in the upcoming years. The goals of this study are to verify the possible differences in the Raman spectra acquired at 852 nm as compared to 785 nm when analyzing a set of different historical pigments frequently encountered during the analysis of polychrome surfaces, and based on the spectral characteristics of the materials, generate a summary to support researchers and conservators in the interpretation of the Raman spectra.

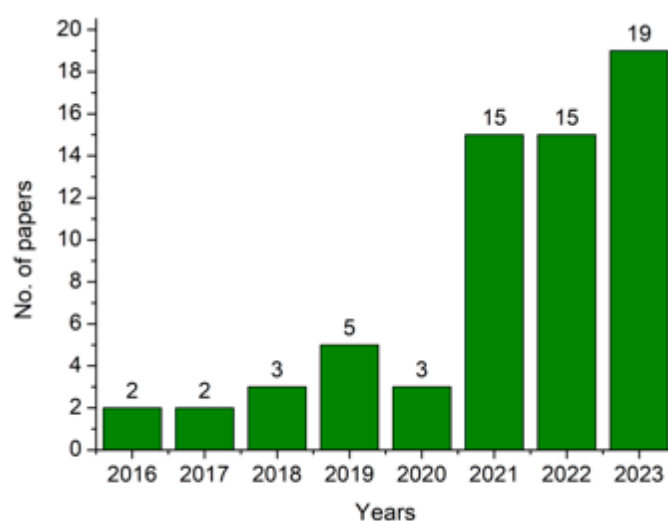


Figure 1. Number of papers exploiting the Bravo spectrometer in heritage science from its marketing year to date.

Additionally, with the aim to verify the applicability of the spectral references of pure pigments using the 852 nm laser excitation wavelength of the Bravo instrument, a mock-up panel painting, prepared in 1995 at the Opificio delle Pietre Dure (Florence, Italy) following the historical recipe for egg-tempera, was analyzed. Also, a comparison with spectra obtained with a 785 nm laser excitation wavelength allowed us to identify changes in the position and relative intensity of the characteristic peaks of some pigments in the spectra obtained with the 852 nm laser excitation wavelength.

2. Materials and Methods

2.1. Samples

A total of 32 pure pigments have been analyzed as dry powder. The analyzed pigments are divided into color categories. Table 2 lists all pigments with additional information. The samples represent a selection of the major pigments utilized in artworks.

Table 2. Analyzed pigments: name and stereoscopic image, chemical composition, color index and number, supplier, and article number. The scale bar shown in the first row is valid for all the images.

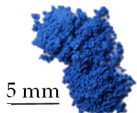
Name and Stereoscopic Image		Chemical Composition [61–63]	Colour Index (C.I.) Name and Number	Supplier and Article Number
Blue pigments	Cobalt blue 	Cobalt(II) oxide–aluminum oxide, cobalt(II) aluminate CoOAl_2O_3 (CoAl_2O_4)	PB28 No. 77346	Kremer, 45710
	Prussian blue 	Iron(III) hexacyanoferrate(II) $\text{Fe}_4[\text{Fe}(\text{CN})_6]_3$	PB27 No. 77510	F.lli Maimeri
	Antwerp blue 	Prussian blue + Cobalt blue	-	n.d.
	Ultramarine blue 	Sodium silicate containing sulfur and aluminum $(\text{Na,Ca})_8[(\text{SO}_4,\text{S,Cl})_2(\text{AlSiO}_4)_6]$	PB29 No. 77007	Kremer, 10500
	Azurite 	Basic copper carbonate $2\text{CuCO}_3 \cdot \text{Cu}(\text{OH})_2$	PB30 No. 77420	Kremer, 10201
	Indigo 	2-(3-oxo-2,3-dihydro-1H-indol-2-ylidene)-2,3-dihydro-1H-indol-3-one $\text{C}_{16}\text{H}_{10}\text{N}_2\text{O}_2$	NB1 No. 75780	Kremer, 36000
	Smalt 	Potassium glass containing cobalt $\text{SiO}_2 + \text{K}_2\text{O} + \text{Al}_2\text{O}_3 + \text{CoO}$	PB32 No. 77365	Kremer, 10010
	Lapis lazuli 	Sodium silicate containing sulfur and aluminum $(\text{Na,Ca})_8[(\text{SO}_4,\text{S,Cl})_2(\text{AlSiO}_4)_6]$	PB29 No. 77007	Kremer, 10530 Origin Afghanistan
	Green earth 	Hydrated iron (II-III) potassium silicate $\text{K}(\text{Mg,Fe}^{2+})(\text{Fe}^{3+},\text{Al})[\text{Si}_4\text{O}_{10}](\text{OH})_2$, and/or $(\text{K,Na})(\text{Fe}^{3+},\text{Al,Mg})_2(\text{Si,Al})_4\text{O}_{10}(\text{OH})_2$	N/A C.I. PG23 No. 77009	Hopkins

Table 2. Cont.

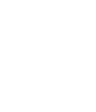
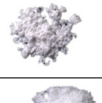
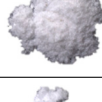
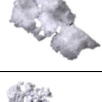
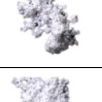
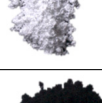
Name and Stereoscopic Image		Chemical Composition [61–63]	Colour Index (C.I.) Name and Number	Supplier and Article Number
Green pigments	Cobalt green 	Cobalt(II) zincate Co_2TiO_4	PG50 No. 77377	Kremer, 44100
	Chromium oxide 	Chromium(III) oxide Cr_2O_3	PG17 No. 77288	Winsor & Newton
	Malachite 	Basic copper (II) carbonate $\text{CuCO}_3 \cdot \text{Cu}(\text{OH})_2$	PG39 No. 77492	Kremer, 10310
	Viridian 	Hydrated chromium(III) oxide $\text{Cr}_2\text{O}_3 \cdot 2\text{H}_2\text{O}$	PG18 No. 77289	Winsor & Newton
Yellow pigments	Massicot 	Orthorhombic lead oxide $\beta\text{-PbO}$	PY46 No. 77577	Kremer, 43010
	Lead tin yellow type I 	Lead(II) stannate Pb_2SnO_4	N/A No. 77629	Kremer, 10110
	Naples Yellow 	Lead (II) antimonate $\text{Pb}_2\text{Sb}_2\text{O}_7$	PY41 No. 77588	Kremer, 13100
	Chrome yellow 	Lead (II) chromate PbCrO_4	PY34 No. 77600	Kremer, 43700
	Cadmium yellow 	Cadmium (II) sulfide, zinc oxide (CdS , ZnO)	PY35 No. 77117	Roberson Ltd.
	Yellow ochre 	Iron(III) oxide–hydroxide $\text{FeO}(\text{OH})$	PBr6 No. 77499	Kremer, 10220
	Raw sienna 	Iron (III) oxide–hydroxide $\text{FeO}(\text{OH})$	PBr6 No. 77491	Winsor & Newton
	Caput mortuum 	Iron (III) oxide Fe_2O_3	PR101 No. 77491	Kremer, 48750
	Umber 	Iron (III) oxide Fe_2O_3	PBr7 No. 77492	Kremer, 40700
	Red bole 	Iron (III) oxide Fe_2O_3	PR102 No. 77015	Kremer, 40503

Table 2. Cont.

Name and Stereoscopic Image		Chemical Composition [61–63]	Colour Index (C.I.) Name and Number	Supplier and Article Number
Red pigments	Cinnabar 	Mercury(II) sulfide HgS	PR106 No. 77766	Kremer, 10600
	Carmin naccarat 	2-Anthracene-carboxylic acid, 7-β-D-glucopyranosyl-9,10-dihydro-3,5,6,8-tetrahydroxy-1-methyl-9,10-dioxo-C ₂₂ H ₂ OO ₁₃	NR4:1 No. 75470	Kremer, 42100
	Alizarin crimson 	Dihydroxy-9,10-anthracene-dione calcium salt (1:1) C ₁₄ H ₈ CaO ₄	PR83 No. 58000:1	Winsor & Newton
White and black pigments	Lead white 	Lead (II) carbonate, basic (PbCO ₃) ₂ ·Pb(OH) ₂	PW1 No. 77597	Kremer 46060
	Gypsum 	Calcium (II) sulfate dihydrate CaSO ₄ ·2H ₂ O	PW25 No. 77231	Kremer, 11800
	Calcite 	Calcium (II) carbonate CaCO ₃	PW18 No. 77220	Merck, 2066
	Barite 	Barium (II) sulfate BaSO ₄	PW22 No. 77120	CarloErba, 425497
	Zinc oxide 	Zinc (II) oxide ZnO	PW4 No. 77947	Merck, 8849
	Ivory black 	Calcium (II) phosphate, calcium (II) carbonate, carbon [Ca ₃ (PO ₄) ₂]+CaCO ₃ +C	Bk9 No. 77267	Winsor & Newton

2.2. Mock-Up Panel Painting

Restorers at Opificio delle Pietre Dure (Florence, Italy) realized the mock-up panel painting in 1995. It was prepared to employ wooden support with a ground layer of rabbit glue and gypsum (CaSO₄·2H₂O) (ratio 1:16 *v/v*) until saturation of the glue, applied with a brush in two steps (the second layer was applied once the first one was completely dry). On top of the ground layer, the imprimatura made of rabbit glue and H₂O in a ratio of 1:32 was applied. Once completed, the prepared surface was divided into sections by drawing slots (1 cm × 3 cm). Egg tempera was prepared by mixing two parts of yolk, one of egg white and one of vinegar. The mock-up panel painting (Figure 2) includes blue pigments such as azurite, indigo, Lapis lazuli, smalt, cobalt blue, Prussian blue, and artificial ultramarine and was investigated using conditions specified in Table 3.



Figure 2. Mock-up panel painting of blue pigments. The pigment is indicated under each square. Azz.: azurite; INDACO: indigo; LAPIS.: Lapis lazuli; Smalt; COB. S.: cobalt blue; PRUS.: Prussian blue; OLT. ART.: ultramarine.

Table 3. Experimental conditions (spectral range, detector integration time, and number of scans) for the samples in powder and mock-up panel painting for the measurement with the pSSE instrument.

	Samples	Spectral Range (cm ⁻¹)	Integration Time (s)	Number of Scans
powders	Cobalt blue	170–1200	2	20
	Prussian blue	170–1200	10	25
	Antwerp blue	170–1200	50	5
	Ultramarine	170–1800	1	30
	Azurite	170–1450	5	20
	Indigo	170–1800	0.5	10
	Smalt	170–1200	5	10
	Lapis lazuli	170–1800		
	Calcite, Barite	170–2000	1	20
	Green earth	170–1200	10	10
	Colbalt green	170–1200	5	10
	Chromium oxide	170–1200	5	5
	Viridian	170–1200	5	15
	Malachite	170–1200	20	5
	Massicot	170–1200	5	5
	Lead tin yellow, Chromium yellow, Cinnabar	170–1200	1	10
	Alizarin crimson	170–1800		
	Naples yellow, Gypsum	170–1200 170–2000	1	5
	Cadmium oxide	170–1200	2	15
	Yellow ochre, Caput mortuum, Umber, Red bole	170–1200	5	15
	Carmin naccarat	170–1800		
	Ivory black	170–2000		
	Raw sienna	170–1200	10	5
Lead white	170–2000	1.5	10	
Zinc oxide	170–1400	1.5	30	
tempera	Azurite	170–1450	5	2
	Indigo Lapis lazuli	170–1800 170–1200	1.5	15
	Smalt	170–1200	1	15
	Cobalt blue	170–1200	1	20
	Ultramarine blue Prussian blue	170–1200 170–2500	1.5	10

2.3. Sequentially Shifted Excitation (SSE) Raman Spectroscopy

The Bravo spectrometer uses a patented technology called SSE™ (Sequentially Shifted Excitation, patent number US8570507B1) to mitigate fluorescence. The device is equipped

with two excitation lasers (DuoLaser™, 785 nm, and 852 nm) that can be temperature-shifted three times over a small wavelength range (about 0.4 nm). Both laser beams impinge on the sample sequentially in every measurement, covering a broad spectral range from 170–2000 cm^{-1} and 2000–3200 cm^{-1} , exploiting the 852 nm and 785 nm lasers, respectively. The laser power was set automatically, reaching a maximum of 100 mW for an 852 nm laser, in an area spot of about $100 \mu\text{m} \times 500 \mu\text{m}$ [45]. In this work, we considered the spectral range 170–2200 cm^{-1} , corresponding to the 852 nm laser excitation, and only the first channel raw data (called CH2) are reported.

The pigment powders were placed on a sheet of aluminum foil, and the Bravo instrument was placed in a vertical position over two aluminum square supports (Figure 3). In this configuration, the laser beam impinges vertically on the pigment powders without any interference.

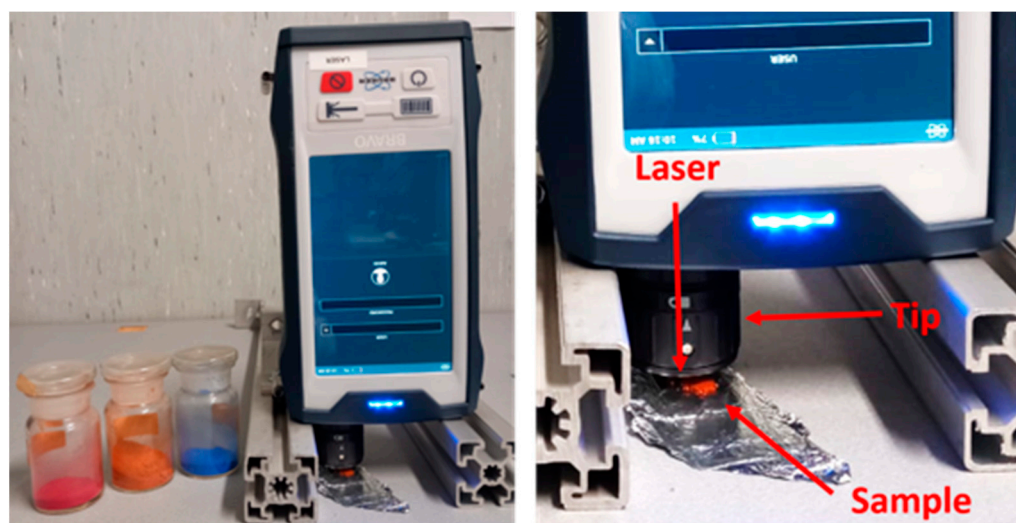


Figure 3. The overall set-up for Raman measurements of pigments placed on a sheet of aluminum (left) and shown in detail (right).

The measurements were first performed with parameters automatically set by the instrument. These are determined by the internal algorithm that evaluates the signal-to-noise ratio. Starting from the so obtained values of integration time, the number of scans was further increased to improve the quality of the obtained spectrum (i.e., 0.5–50 s detector integration time and 5–30 accumulations—Table 3) depending on the response of the investigated materials.

2.4. Micro-Raman Renishaw (785 nm)

A benchtop Raman confocal microscope (Renishaw inVia) equipped with a Leica DM2700 optical microscope was employed to acquire micro-Raman spectra using a 785 nm excitation diode laser. We performed the measurement in the spectral range 170–1800 cm^{-1} , using a grating 1200 lines/mm and a thermoelectrically cooled CCD pixel (functional resolution 400–1060 cm^{-1}). The laser powder was kept below 7 mW, using a 10 s exposure time and 5 accumulations.

2.5. Stereomicroscopy

The powder pigments were examined under a Leica M205C stereomicroscope with a camera Leica DFC 295 at 0.78 \times . White balance over a white surface was performed before capturing the images that were processed with LAS v4.6 software.

3. Results

Raman spectra acquired with an 852 nm laser excitation wavelength of each pigment are reported here. The results are conventionally organized into sections according to the

pigments' color as follows: 3.1 blue, 3.2 green, 3.3 yellow, 3.4 red, and 3.5 white and black pigments. A summary of the peaks' assignment with relevant references is reported in Table A1 of Appendix A. The Raman spectra obtained also with 785 nm laser excitation wavelength are reported for comparison (in green lines) only when notable differences in Raman peak position/intensity or spectral shape have been encountered.

3.1. Blue Pigments

The 852 nm Raman spectra of eight blue pigments—cobalt blue, Prussian blue, Antwerp blue, ultramarine, azurite, indigo, smalt, and Lapis lazuli—are displayed respectively in Figure 4a–h. For Cobalt blue, smalt, and Lapis lazuli, some differences between 852 and 785 nm-generated Raman spectra were detected; therefore, comparative spectra are reported in Figure 4a,e,f.

Cobalt blue ($\text{CoO}\cdot\text{Al}_2\text{O}_3$, Figure 4a) is detected by the bands positioned at 204 cm^{-1} (Co-O tetrahedral sites vibrational), 410 cm^{-1} (symmetric bending of AlO_4), 514 cm^{-1} (asymmetric stretching of AlO_4), 615 cm^{-1} (antisymmetric stretching of AlO_4), and 754 cm^{-1} (symmetric stretching vibration of the AlO_4) within the spinel lattice [64]. As compared to the spectrum with the 785 nm laser excitation line (Figure 4a, green line), the number of bands and their positions are the same; however, their intensities at the low wavenumbers are inverted, being the ratio $204/410\text{ cm}^{-1}$ lower for the 852 nm laser.

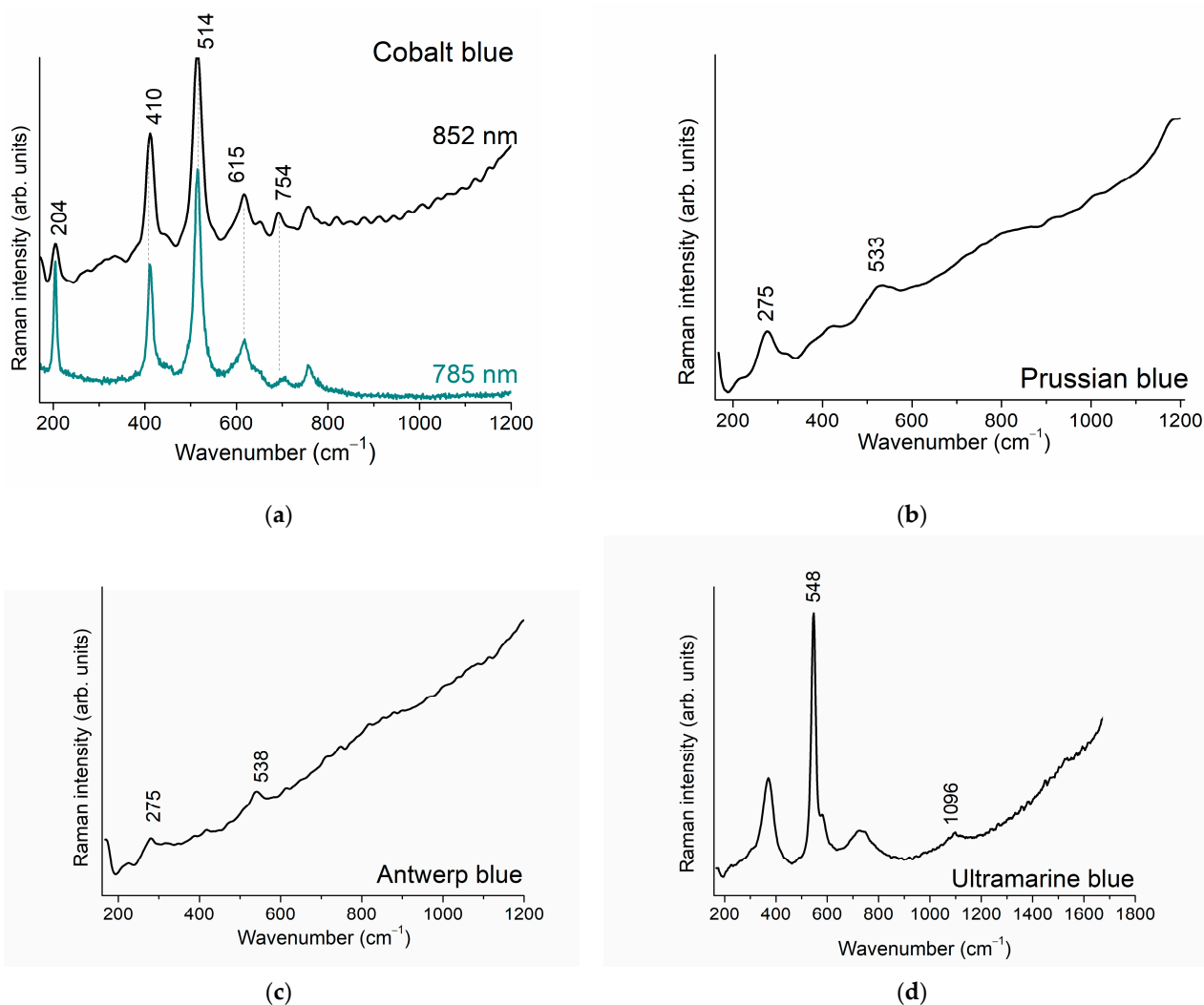


Figure 4. Cont.

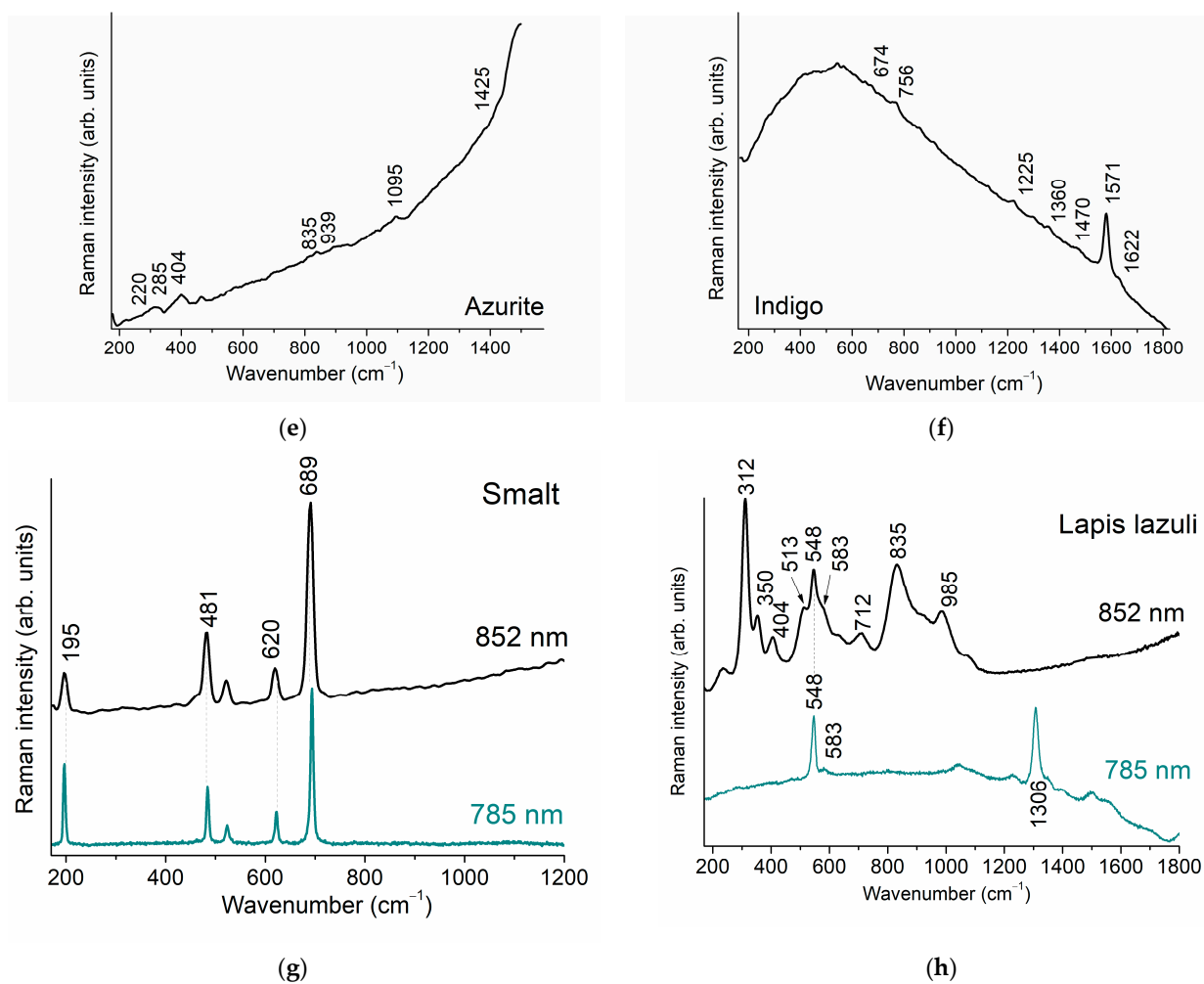


Figure 4. Raman spectra of blue pigments: (a) cobalt blue, (b) Prussian blue, (c) Antwerp blue, (d) ultramarine, (e) azurite, (f) indigo, (g) smalt, and (h) Lapis lazuli. All the Raman spectra acquired with 852 nm laser excitation wavelength are reported in black lines, while those acquired with 785 nm in green lines (a,g,h).

The Raman spectrum of Prussian blue (Figure 4b) is detected by the two low-frequency bands located at 275 cm^{-1} and 538 cm^{-1} due to Fe-CN-Fe deformation vibration and Fe-C stretching vibration, respectively [65]. The major bands of Prussian blue, positioned at 2090 and 2159 cm^{-1} ($\text{C}\equiv\text{N}$ stretching vibration), are absent in the 852 nm generated spectrum owing to the detection range limits; however, they can be detected by the other 785 nm laser excitation wavelength of instrumentation (not reported in Figure 4b).

Antwerp blue (Figure 4c) is a combination of Prussian blue and Cobalt blue [66]. The Raman spectra obtained with 852 nm laser excitation wavelength highlight only the presence of Prussian blue for the two low-frequency bands located at 275 and 533 cm^{-1} , and no information about the presence of cobalt blue was detected [65].

Ultramarine (Figure 4d), a synthetic pigment of an approximate formula $\text{Na}_{6-10}\text{Al}_6\text{Si}_6\text{O}_{24}\text{S}_{2-4}$, is identified by its principal band at 548 cm^{-1} (and its shoulder at 585 cm^{-1}) due to the symmetric stretching mode of S^{3-} in the sulfur-containing sodium-silicate pigment. Its first overtone at 1096 cm^{-1} is also detected [67].

The overall intensity and quality of the Raman spectrum of azurite at 852 nm is low (Figure 4e). In agreement with the spectra obtained at 785 nm, it is characterized by a band placed at 404 cm^{-1} (lattice mode), by the bands related to the symmetric and asymmetric stretching of carbonate at 1095 cm^{-1} and 1425 cm^{-1} , respectively, and by the symmetric bending mode detectable at 835 cm^{-1} . Low-intensity bands present at lower frequencies

are assigned to lattice modes (220 and 284 cm⁻¹). Furthermore, the out-of-plane bending mode of the OH group present in the azurite molecule is located at 939 cm⁻¹ [68]. In the considered spectral range, however, it is not possible to detect the bands at 3427 and 3453 cm⁻¹ assigned to the hydroxyl-stretching modes of the OH unit of azurite [69].

The characteristic Raman bands of indigo (Figure 4f) are placed at 674 cm⁻¹, 756 cm⁻¹, 1225 cm⁻¹ (rocking vibration of N-H), 1470 cm⁻¹ (rocking of C-H), and 1360, 1571, and 1622 cm⁻¹ (stretching vibration of conjugate system C=C, C=O, and N-H group) [70], the last two being the most intense.

The Raman spectrum of smalt (Figure 4g) is dominated by the intense band assigned to the Si-O-Si vibration mode of silicate at 689 cm⁻¹ [71], and the lower frequencies are assigned to the breathing vibration mode of the T-O-T substructure and correlate with the size of the TO₄ tetrahedra ring, where T = Si or Al [72]. Similarly to Cobalt blue, as compared to the spectrum with a 785 nm laser excitation line (Figure 4g, green line), the band intensities at the low wavenumbers are inverted, being the 195/481 cm⁻¹ ratio lower for the 852 nm laser.

Lapis lazuli, as ultramarine, is detected by the band at 548 cm⁻¹ and a shoulder at 583 cm⁻¹ (Figure 4h) attributed to lazurite S₃⁻ and S₂⁻ symmetric stretching mode. On the contrary to the spectrum of the artificial pigment (Figure 4c) and to that obtained with 785 nm (Figure 4h), this spectrum obtained through 852 nm laser excitation wavelength is very complex and characterized by several sharp and broad bands (namely at 312 vs, 350 m, 405 w, 513 m, 712 w, 835 s, 985 m), not correlated directly to lazurite. This spectral behavior is probably due to luminescence phenomena. In general, the activators of luminescence phenomena—including rare earth elements, Fe²⁺, Fe³⁺, Co²⁺, and Ni²⁺—are chemical impurities in the mineral structure. The 785 nm laser excitation wavelength Raman spectrum gave rise to two sharp bands, one related to lazurite (548 cm⁻¹) and the luminescent band at 1306 cm⁻¹ attributed to the presence of diopside [73]. González-Cabrera et al. [74] exploit these luminescence phenomena to discriminate natural from synthetic ultramarine blue. Other researchers [75,76] link these wavelength-dependent luminescence spectral patterns to the geographical provenance of the samples. It is most likely that the observed luminescent pattern at 852 nm laser excitation wavelength is associated with diopside; however, more in-depth research is necessary to explore its precise origin.

To showcase a different pigment spectral behavior under different laser excitation wavelengths, the example of Lapis lazuli is reported in Table 4. Lapis lazuli is detected by the band at 548 cm⁻¹ referred to mineral of lazurite in the spectra acquired with all the laser excitation wavelengths. The spectra generated with 532 nm and 638 nm laser excitation wavelengths, in addition to 260 cm⁻¹ and 548 cm⁻¹ (bending and stretching of S₃⁻ ion, respectively), also show overtone bands (548 × 2 = 1096 cm⁻¹, 548 × 3 = 1644 cm⁻¹, etc.) or combinations [260 + 548 = 808 cm⁻¹; 260 + (2 × 548) = 1358 cm⁻¹; etc.]. The shoulders at ca 258 and 583 cm⁻¹ correspond to asymmetric modes of lazurite. This Raman fingerprint is typical of resonance Raman spectra of lazurite [77].

Table 4. Peak frequencies and their relative intensities of Lapis lazuli under different laser excitation wavelengths.

Measured Peaks (cm ⁻¹) in This Work Lapis Lazuli Kremer #10530			References Peaks (cm ⁻¹) [9] Lapis Lazuli Kremer #10510		
785 nm	852 nm	532 nm	638 nm	785 nm	1064 nm
		260 m	260 m		
		285 sh	285 sh		
	312 vs *				
	350 m *				

Table 4. Cont.

Measured Peaks (cm ⁻¹) in This Work Lapis Lazuli Kremer #10530		References Peaks (cm ⁻¹) [9] Lapis Lazuli Kremer #10510			
405 w *					
513 m *					
				364 m	364 m
548 s	548 s	548 vs	548 vs	548 vs	548 s
583 vw	583 sh	583 sh	583 sh	583 m	
712 w *					
		808 w	808 w		
835 s *					
985 m *					
		1096 m	1096 m		
1306 s *		1346 m			
		1358 vw	Split into two bands		
		1644 m	1644 m		

v: very; s: strong; m: medium; w: weak; * luminescence phenomena.

Other laser excitation wavelengths, i.e., 785 nm, 852 nm, and 1064 nm, do not generate resonance Raman spectra and exhibit a lower number of bands. The Raman spectrum acquired with 1064 nm laser excitation wavelength is very noisy, and only 364 cm⁻¹ and 548 cm⁻¹ peaks are detected.

3.2. Green Pigments

Five green pigments—green earth, cobalt green, chromium oxide, malachite, and viridian—were analyzed. The 852 nm laser excitation spectra are reported in Figure 5a–e. Spectra with 785 nm are reported for green earth (Figure 5a) and viridian (Figure 5d).

Raman spectrum of green earth (Figure 5a) is characterized by several broad bands that cover the spectral range of 200–550 cm⁻¹. The Raman bands centered at 200 and 277 cm⁻¹ are due to internal vibrations of the MoO₆ octahedra, where Mo is the inter-layer metal atom, and those located at 393 and 533 cm⁻¹ are the bands mainly due to the vibrational modes of the SiO₄ tetrahedra [20]. These bands indicate the presence of celadonite, as the main mineral component of green earth. In these spectra, because of the natural origin of the pigment, Raman bands of gypsum are also present (1006 and 1135 cm⁻¹) [78]. By changing the excitation to 785 nm (Figure 5a, green line), an apparent shift towards higher wavenumbers of the 533 cm⁻¹ band is observed (the shift is from 533 to 547 cm⁻¹), probably due to intensity changes in an unresolved doublet. Similar behavior was previously reported by Ospitali et al. when changing the excitation from 514.5 to 780.0 nm [79].

Cobalt green (Figure 5b)—Co₂TiO₄—is characterized by an intense band at 713 cm⁻¹ (symmetric stretching of CoO₆ octahedra in CoTiO₃) [20], and other bands are at 520, 460, and 340 cm⁻¹. The major bands of chromium oxide (Figure 5c) are positioned at 297, 350, 528, 615 cm⁻¹ (bending mode CrO₃), and 554 cm⁻¹ (symmetric stretching of Cr₂O) [80].

Viridian (Figure 5d) is a mixture of anhydrous and hydrated chromium oxides, as the recorded Raman bands at 487 and 584 cm⁻¹ are attributed to the hydrated oxide and that at 262 cm⁻¹ to the anhydrous one [81]. On the other hand, the spectrum obtained with 785 nm laser excitation wavelength yields a large fluorescence background and accompanying noise; therefore, its identification is not possible.

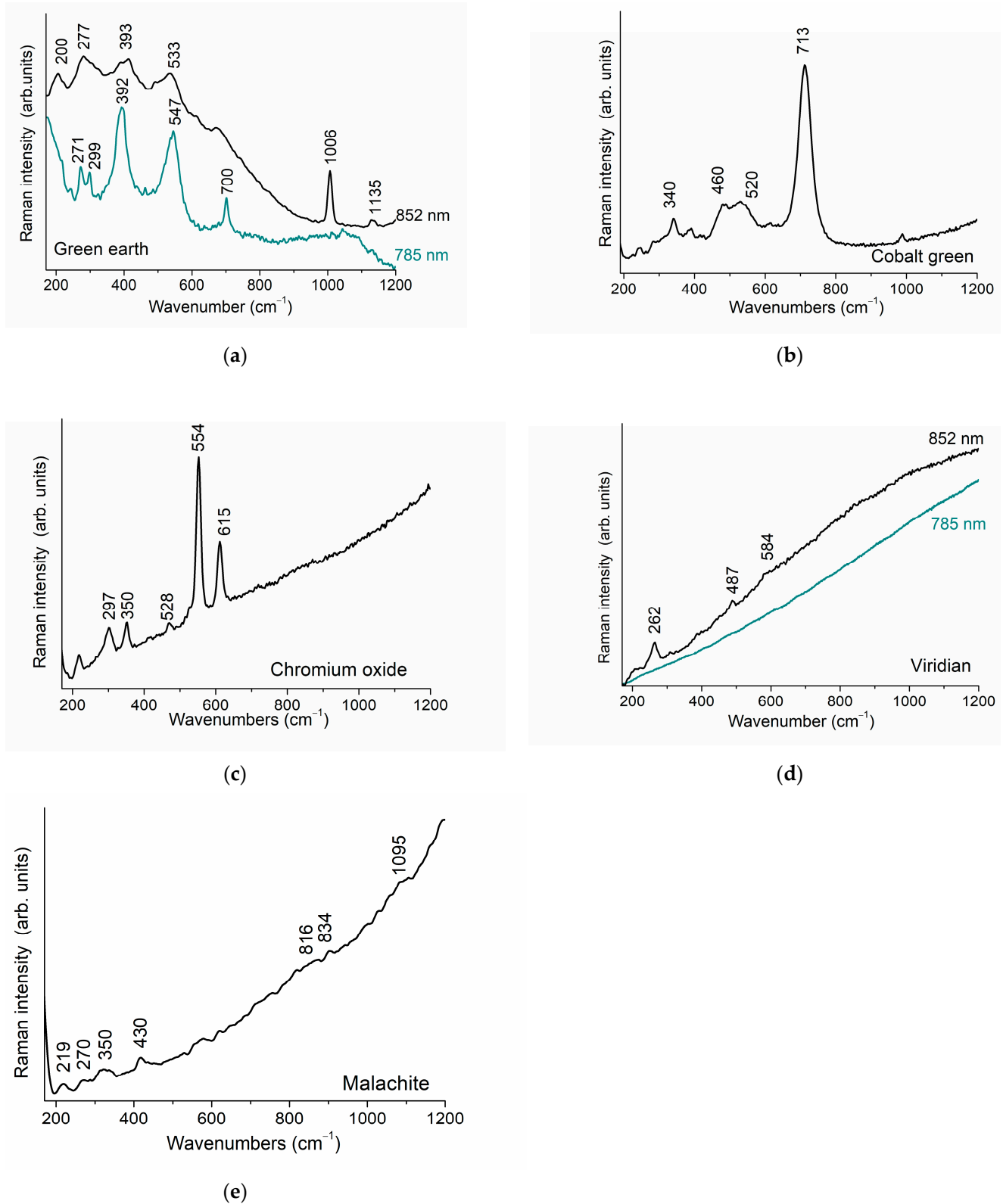


Figure 5. Raman spectra of green pigments: (a) green earth, (b) cobalt green, (c) chromium oxide, (d) viridian, and (e) malachite. Raman spectra acquired with 852 nm laser excitation wavelength are reported in black lines, while those with 785 nm are in green lines (a,d).

Malachite (Figure 5e) is detected by the band at 430 cm^{-1} , together with the peaks at 219, 270, and 350 cm^{-1} that are related to lattice modes and bands due to symmetric stretching (1095 cm^{-1}) and symmetric bending mode (816 and 834 cm^{-1}) of CO_3^{2-} [69]. In

this spectrum, unlike the one from azurite, the band at 1425 cm^{-1} (asymmetric stretching vibration) is not detected, and hence, the spectral range reported is cut off at 1200 cm^{-1} .

3.3. Yellow Pigments

The 852 nm Raman spectra of six yellow pigments investigated—massicot, lead–tin yellow type I, Naples yellow, chromium oxide, cadmium yellow, yellow ochre, and raw sienna—are reported in Figure 6a–g. No significant spectral changes are recorded compared with the 785 nm laser excitation wavelength.

In general, the low wavenumber region provides a confident recognition of massicot (PbO); in particular, the major band at 142 cm^{-1} (symmetric stretching of Pb–O) [45] is not detected by the Bravo instrument due to limited spectral region ($>170\text{ cm}^{-1}$). However, the diagnostic bands of massicot at 290 and 385 cm^{-1} are well discerned (Figure 6a).

Lead–tin yellow type I (Pb₂SnO₄) spectrum (Figure 6b) at 852 nm is well characterized by the bands at 197, 275, 290, 455, and 524 cm^{-1} . The main band of lead–tin yellow at 130 cm^{-1} (due to symmetric stretching vibration of Pb–O) [82] is out of the detectable spectral range of the instrument. No significant differences as compared to 785 nm were observed.

Naples yellow (Pb₂Sb₂O₇) (Figure 6c) has a typical spectral pattern in the 200–400 cm^{-1} spectral region (290, 318, and 348 cm^{-1}) of the vibrational mode of both Sb–O and Pb–O bonds; instead, the band at 510 cm^{-1} is due to Sb–O stretching of the SbO₆ octahedra [83]. Other characteristic bands of Naples yellow are placed at 440 and 613 cm^{-1} .

Chrome yellow (PbCrO₄, crocoite, Figure 6d) is detected by the Raman instrument at 852 nm, unveiling the most informative 774–942 cm^{-1} spectral range related to symmetric stretching of the Cr–O bond [45] detected at 841 cm^{-1} , together with the bands around 360 cm^{-1} .

Cadmium yellow (CdS, ZnO) (Figure 6e) is characterized by the bands at 298 and 597 cm^{-1} assigned to the longitudinal optic phonon (LO) + 2E₂ and the overtone 2LO + 2E₂ of the CdS crystal lattice [84]. The band at 212 cm^{-1} is related to the longitudinal acoustic (LA) phonon modes of the ZnS crystal lattice [85]. The unlabeled bands at 987 cm^{-1} and 457 cm^{-1} correspond to the symmetric stretching mode of barite SO₄ tetrahedra, probably added as a filler.

Yellow ochre and raw sienna (Figure 6f,g)—which are mainly constituted by goethite chromophore—are detected by bands placed at 300 cm^{-1} (Fe–OH symmetric bending), 387 cm^{-1} (Fe–O–Fe/–OH symmetric stretching), and 549 cm^{-1} (Fe–OH asymmetric stretching) [86]; in addition, the gypsum bands are present (1008 and 1134 cm^{-1}).

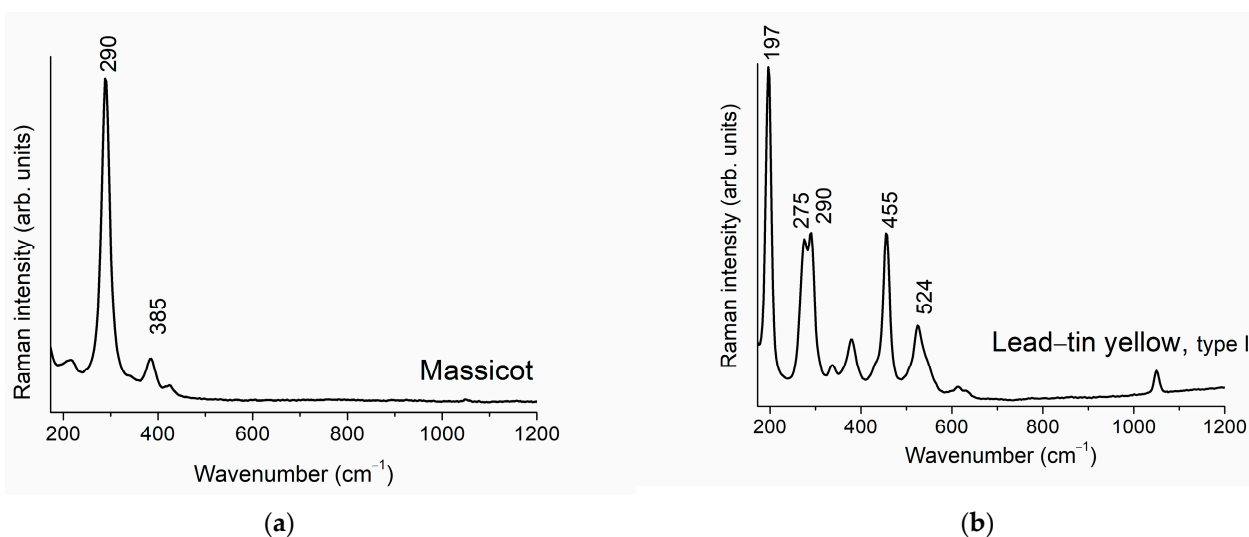


Figure 6. Cont.

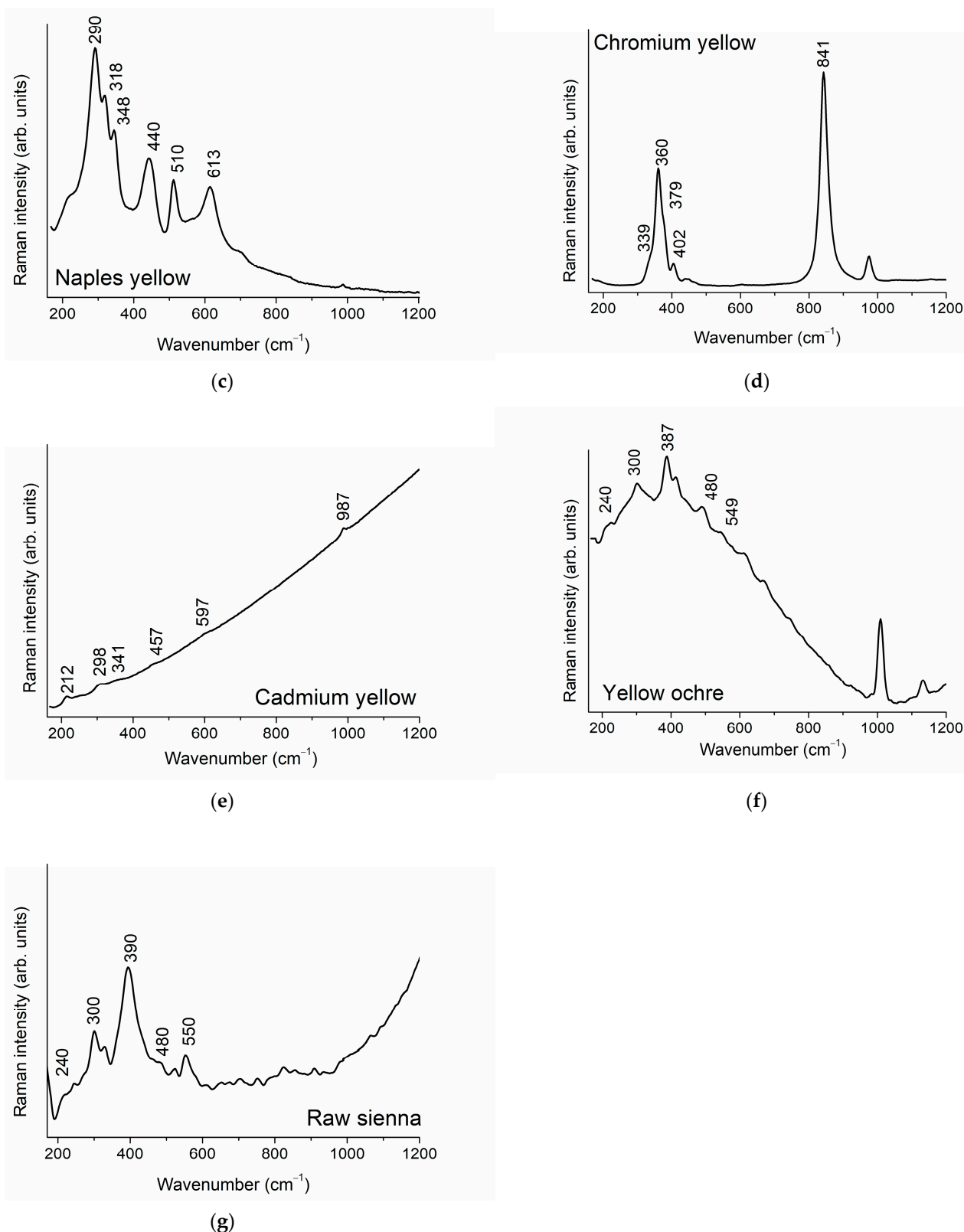


Figure 6. Raman spectra of yellow pigments: (a) massicot, (b) lead–tin yellow type I, (c) Naples yellow, (d) chromium yellow, (e) yellow ochre, (f) raw sienna, and (g) raw sienna.

3.4. Red Pigments

The 852 nm Raman spectra of six red pigments—caput mortuum, umber, red bole, cinnabar, Carmin naccarat, and Alizarin crimson—are reported in Figure 7a–f. As for the

yellow pigments, also the Raman spectra of red pigments at 852 nm are very similar to those generated with a 785 nm laser.

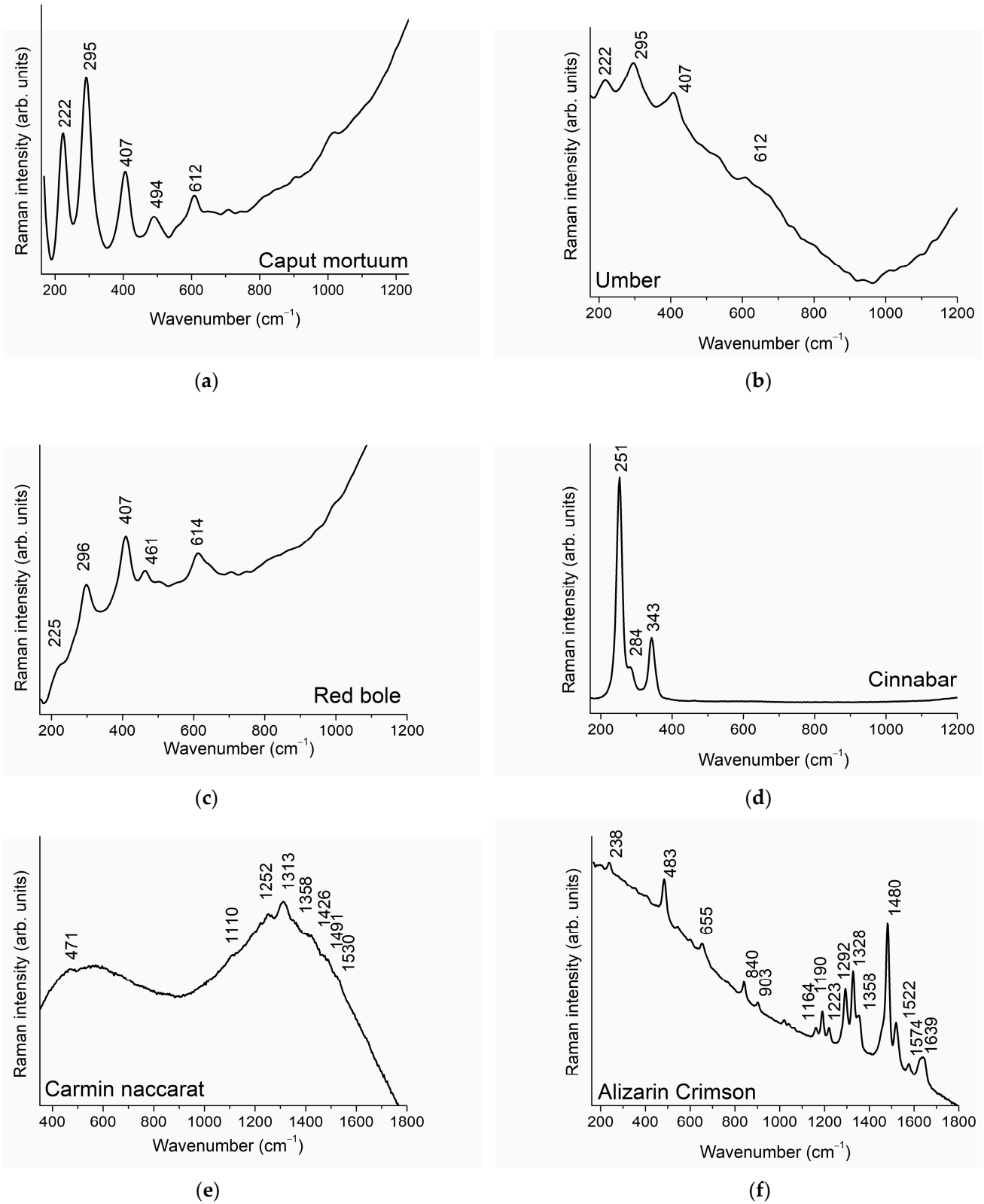


Figure 7. Raman spectra of red pigments: (a) caput mortuum, (b) umber, (c) red bole, (d) cinnabar, (e) Carmin naccarat, and (f) Alizarin crimson.

Caput mortuum, umber, and red bole are detectable through their major intensity bands related to iron oxides modes placed at 222 and 494 cm^{-1} (symmetric stretching vibration of Fe-O), 295 and 612 cm^{-1} (symmetric bending of Fe-O), and 407 cm^{-1} (symmetric stretching of Fe-O-Fe/-OH) [45]. While caput mortuum and umber (Figure 7a,b) have the same spectral trend in terms of relative intensity between the bands, being the band at 295 cm^{-1} the most intense, the major band of red bole (Figure 7c) is that at 407 cm^{-1} .

The Raman spectrum of cinnabar (Figure 7d) is characterized by a very intense band at 251 cm^{-1} with a shoulder at 284 cm^{-1} , and a band at 343 cm^{-1} is also present. These bands are assigned to HgS stretching modes and are orientation-dependent [87].

Carmin naccarat (Figure 7e), an aluminum lake of carminic acid, also known as cochineal lake, is detectable by the bands placed at 471 cm^{-1} (skeletal vibrations); 1110 and 1530 cm^{-1} ($\delta(\text{OH}) + \delta(\text{CH})$); 1250, 1358, 1426 cm^{-1} (Gly); 1312 cm^{-1} ($\delta(\text{OH}) + \delta(\text{CH}) + \delta(\text{ring})$); 1491 cm^{-1} ($\delta(\text{CH}(\text{m}))$) [88].

Raman spectrum of Alizarin crimson (Figure 7f) is characterized by bands placed at 1480, 1328, and 1292 cm^{-1} and other characteristic bands at 238, 483, 655, 840, 903, 1020, 1047, 1164, 1190, 1223, 1358, 1522, 1574, and 1639 cm^{-1} .

3.5. White and Black Pigments

The spectra of the five white pigments investigated—lead white, gypsum, calcite, barite, and zinc oxide—are reported in Figure 7a–d together with that of ivory black (Figure 7f). Lead white ($\text{PbCO}_3)_2 \cdot \text{Pb}(\text{OH})_2$ (Figure 8a) is detected by the Raman band at 1051 cm^{-1} (symmetric stretching of CO_3^{2-} ion) [89] and by the bands at 1365 and 1484 cm^{-1} due to asymmetric stretching mode of CO_3^{2-} [68]. Other lower-intensity bands are placed at 329, 417, and 681 cm^{-1} .

Raman spectrum of selenite (Figure 8b), a variety of gypsum, is characterized by intense bands at 1008 cm^{-1} (symmetric stretching of SO_4^{2-} group) and 1133 cm^{-1} (asymmetric stretching mode of SO_4^{2-}). Bands at 316 cm^{-1} (translational mode of H_2O , Ca) [78], 413 and 495 cm^{-1} (δSO_4^{2-}), and 620 and 674 cm^{-1} (ν_4 , SO_4) are also observed [78].

Raman spectrum of calcite (CaCO_3) (Figure 8c) is characterized by the band placed at 285 cm^{-1} due to external vibration of the CO_3^{2-} groups that involve translator oscillations of these groups (relative translation between cation and anionic group) and by the band at 1089 cm^{-1} due to symmetric stretching of CO_3^{2-} . Even the bands at 714 cm^{-1} (ν_4 , CO_3^{2-}) and 1437 cm^{-1} (ν_3 , CO_3^{2-}) are present in the Raman spectra of calcite [68].

Barite (BaSO_4) (Figure 8d) is identified by intense Raman bands at 989 cm^{-1} and 460 cm^{-1} symmetric stretching of SO_4^{2-} ; 619 and 644 cm^{-1} (asymmetric bending of SO_4^{2-}); 1079, 1105, 1141, and 1166 cm^{-1} (asymmetric stretching of SO_4^{2-}) [90].

Raman band at 440 cm^{-1} is characteristic of zinc oxide (ZnO) (Figure 8e), together with 336 and 581 cm^{-1} . Bands at 1082 and 1156 cm^{-1} are assigned to the second-order Raman spectrum arising from zone boundary phonons [91].

In the Raman spectrum of Ivory black ($[\text{Ca}_3(\text{PO}_4)_2] + \text{CaCO}_3 + \text{C}$) (Figure 8f), a carbon black pigment is detected by a couple of broad bands at 1336 and 1600 cm^{-1} ; the former (C-C D1 band) is assigned to edge effect, plane defects, and heteroatoms as oxygen or double bonds. Other impurities are considered responsible for this broad band. The D1 band position is found to cover the whole range of 1240 to 1400 cm^{-1} , and the C-C D2 band at 1600 cm^{-1} is assigned to C-C in-plane symmetrical stretching [19]. Notably, the 961 m ($\nu_1(a_1) \text{PO}_4^{3-}$) is not observed. The broad bands characterizing carbon-black pigments are occasionally subtracted by PCA pSSE elaboration, which has proven slightly inefficient [45]. As a result, it is always recommended to view the raw spectra. In this spectrum, a band at 1475 cm^{-1} marked with an asterisk is due to an internal optical contribution of the employed instrumentation.

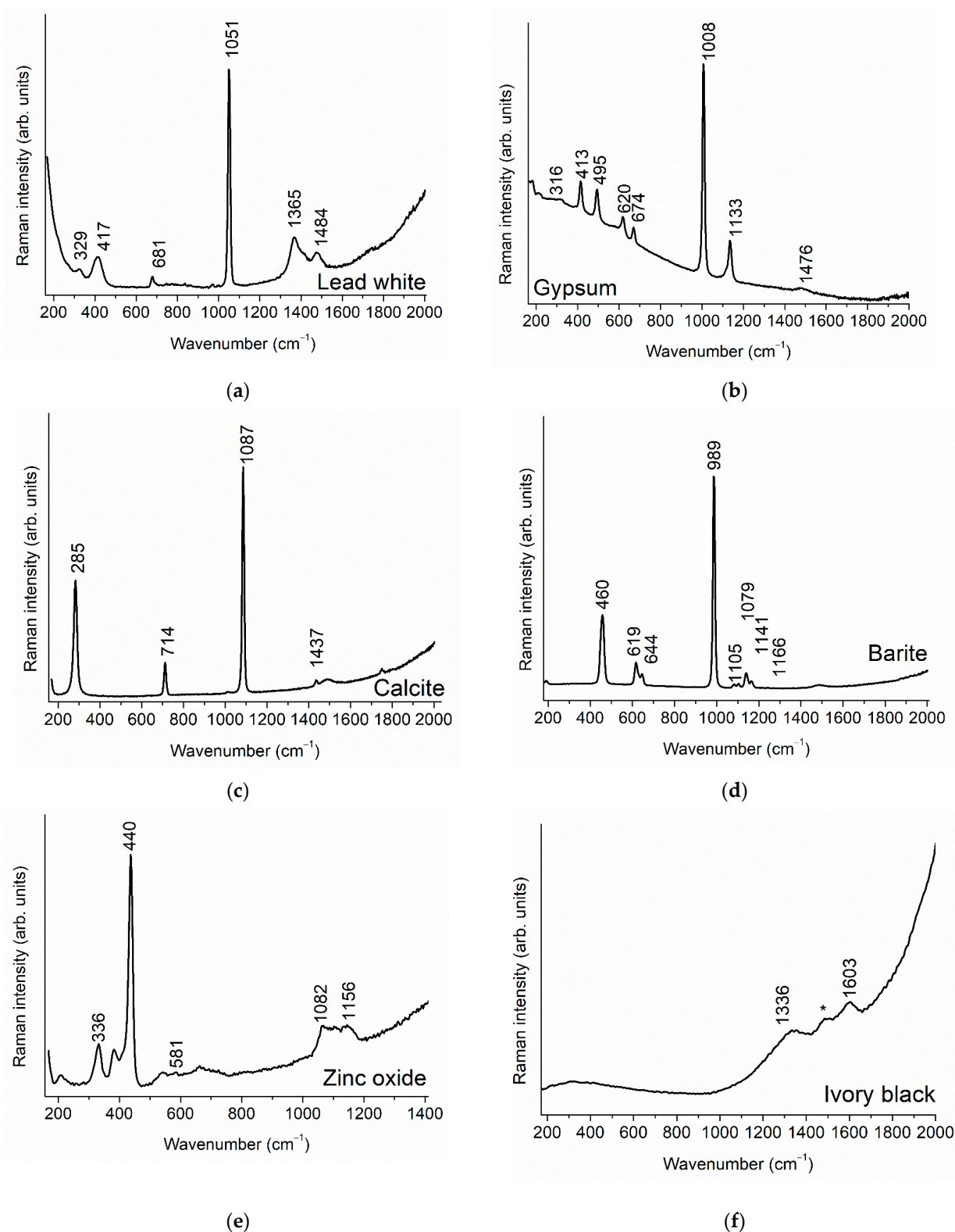


Figure 8. Raman spectra of white and black pigments: (a) lead white, (b) gypsum, (c) calcite, (d) barite, (e) zinc oxide, and (f) ivory black. The asterisk indicates a band due to the glass of the tip.

4. Mock-Up Panel Painting

To test the applicability of the 852 nm laser excitation wavelength of the Bravo instrument in possible real cases, a wooden panel tempera painting with blue pigments (Figure 2) was analyzed. Raman spectra (raw CH_2) acquired directly on the mock-up

panel painting are compared with reference powder pigments in Figure 9, showing a good spectral correspondence.

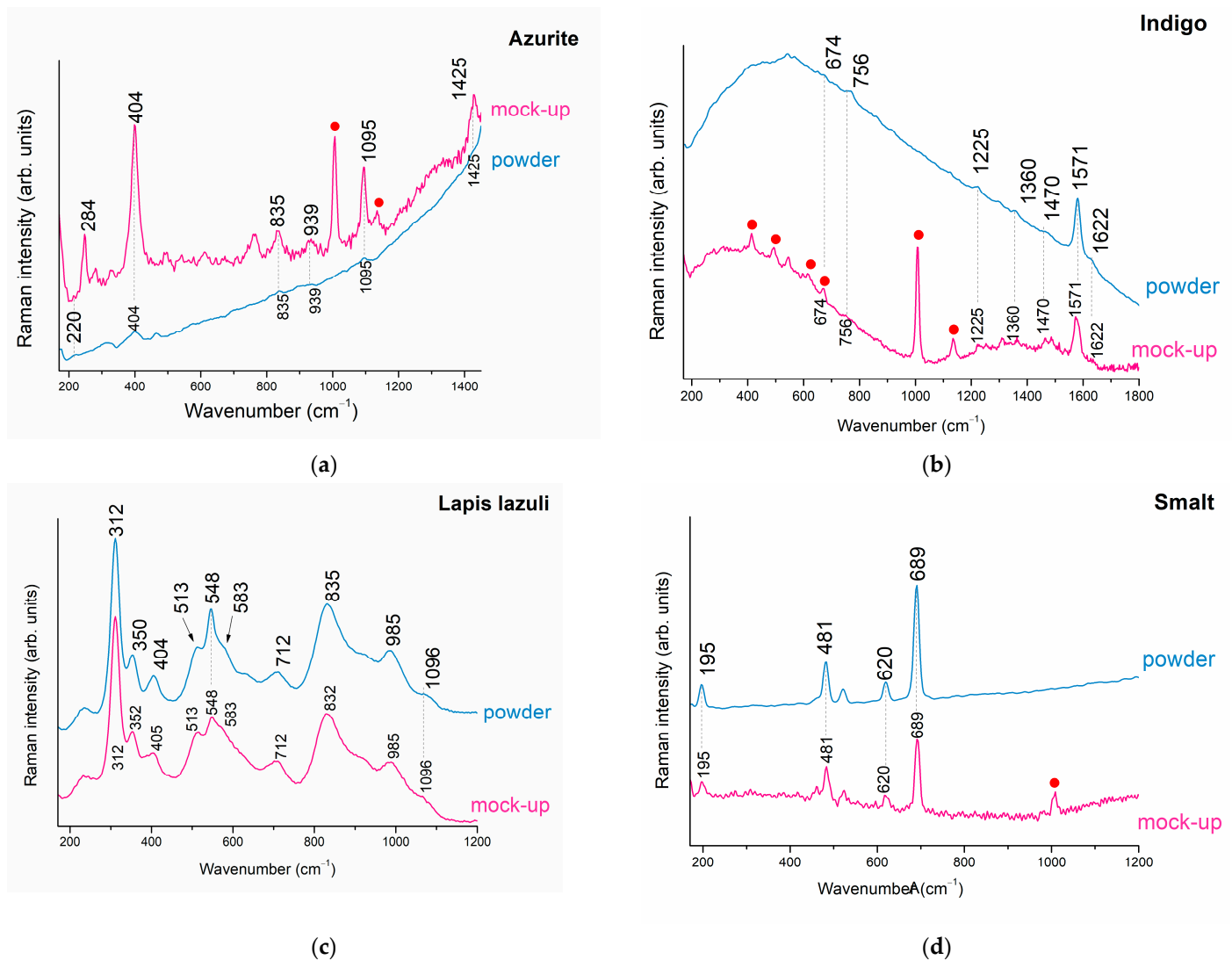


Figure 9. Raman spectra of blue pigments in mock-up panel painting: (a) azurite, (b) indigo, (c) lapis lazuli, and (d) smalt. Pink lines (named mock-up) indicate the Raman spectra acquired on mock-up panel painting, and cyan lines (named powder) refer to Raman spectra of pigments in powder. All the spectra are acquired with an 852 nm laser excitation wavelength.

The azurite paint layer (Figure 9a) is characterized by the main bands at 404 and 320 cm^{-1} , the spectrum obtained from the mock-up being more intense. Indigo (Figure 9b) in the mock-up is detected by its major band at 1571 cm^{-1} , and the spectrum is dominated by the bands of gypsum (marked with red dots in the spectrum) from the ground layer.

The spectrum of Lapis lazuli (Figure 9c) is characterized by the band of lazurite at 548 cm^{-1} . Other photoluminescence signals are observed as discussed earlier (Figure 4h). The results obtained from the smalt paint layer (Figure 9d) contain all the characteristic bands of the pigments in addition to those arising from the preparation layer.

Among all the spectra registered from the paint model, the spectrum from cobalt blue (Figure 10a) is the most challenging to interpret because the bands from the pigment are located in proximity to the characteristic peaks arising from gypsum in the ground layer. Despite this inconvenience, it is possible to identify the peaks of cobalt blue.

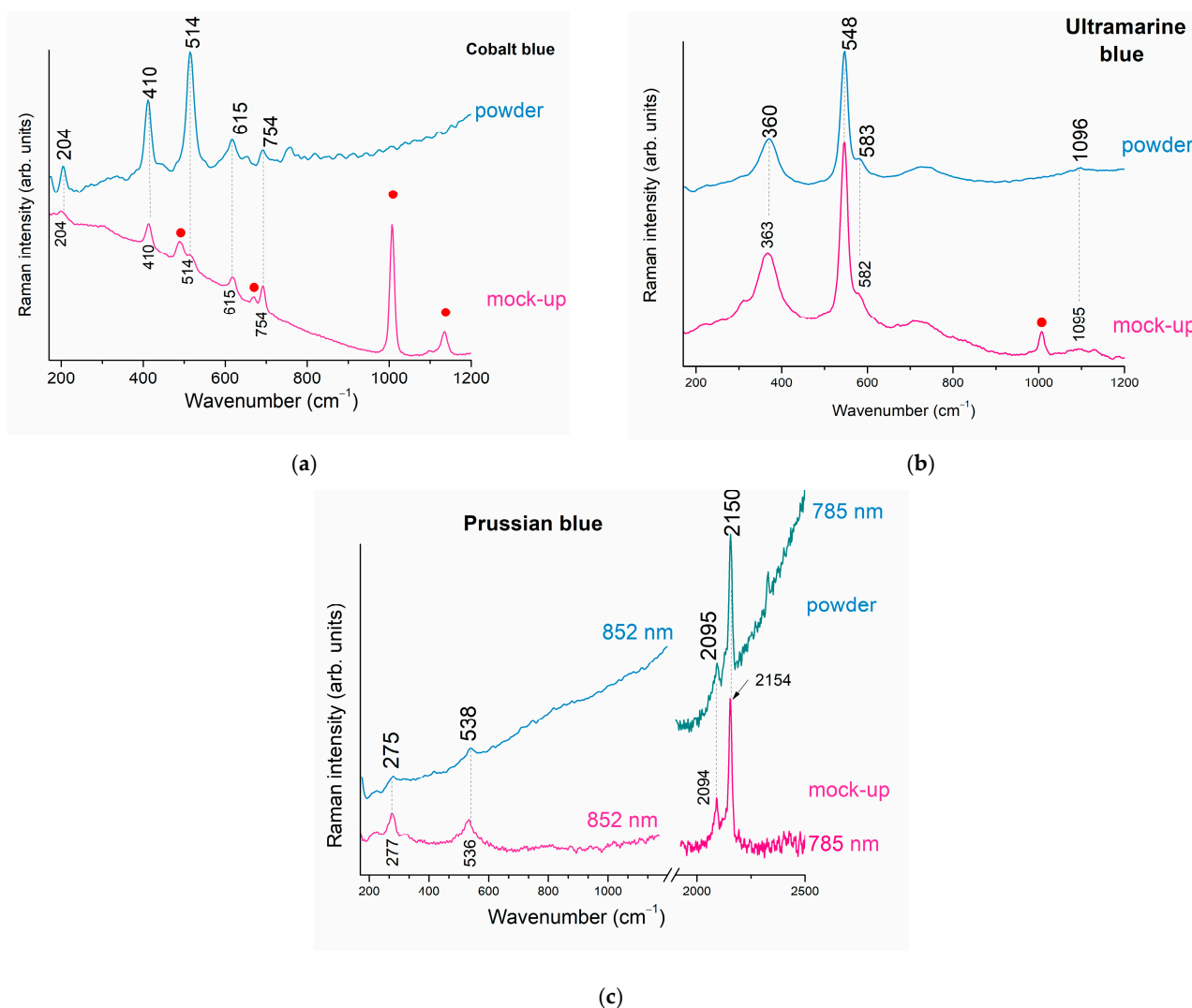


Figure 10. Raman spectra of blue pigments in mock-up panel painting: (a) cobalt blue, (b) ultramarine blue, and (c) Prussian blue (spectral range 170–2500 cm^{-1}). Pink lines (named mock-up) indicate the Raman spectra acquired on mock-up panel painting, and cyan lines (named powder) refer to the Raman spectra of pigments in powder. All the spectra are acquired with an 832 nm laser excitation wavelength, and Prussian blue is also acquired with a 785 nm laser excitation wavelength.

Ultramarine pigment (Figure 10b) is well detected in the mock-up by the band at 548 cm^{-1} ; interestingly, the spectrum is free from the photoluminescence phenomena as observed earlier for pigment powder. For the Prussian blue layer, the entire spectrum (obtained by merging the spectra from 852 nm and 785 nm excitation laser) is reported in Figure 10c. In fact, the major bands of Prussian blue are placed at 2095 and 2150 cm^{-1} , as observed for both the mock-up and the pigment powder.

5. Conclusions

The creation and the availability of a spectral database of reference materials are crucial to enable conservation scientists to rapidly identify and study unknown pigments commonly employed in artworks. This work provides the Raman spectra of 32 pigments of historic and artistic importance acquired at 852 nm laser excitation wavelength. This wavelength proved suitable for the detection of all the pigments investigated even though some of them present a strong fluorescence background. Indeed, despite the weak signal in the Raman spectra of azurite, malachite, viridian, and cadmium yellow, their identification possibly outperforms the 785 nm laser excitation wavelength in some cases.

Some differences in the spectral shape and relative intensity of the Raman peaks between spectra obtained with 852 nm and 785 nm laser excitation wavelength were detected for some blue and green pigments. The results suggest that the spectra of pigments such as cobalt blue and smalt exhibit inversions in the relative intensity of the bands at low wavenumbers. An interesting case is represented by Lapis lazuli that upon 852 nm laser wavelength excitation produces a characteristic photoluminescence pattern that differs from that of synthetic ultramarine. The comparison between the two laser excitation wavelengths also highlighted the main advantage of using longer wavelengths for the detection of viridian. The 785 nm spectra of viridian are completely masked by fluorescence; while with 852 nm laser excitation wavelength, the main bands are detectable.

Among the aspects to be considered is the covered spectral range by the 852 nm excitation laser ($170\text{--}2000\text{ cm}^{-1}$) that excludes the main bands of some pigments, e.g., Prussian blue, massicot, and lead–tin yellow. Anyway, the presence of the other characteristic bands of each pigment leads to their identification. Also considering the 785 nm excitation laser employed by Bravo, the spectral range is extended to 3200 cm^{-1} enabling to identify the Prussian blue uniquely.

Our future prospects concern the expansion of this online database with other natural and synthetic pigments as well as organic dyes.

Author Contributions: Conceptualization, J.S.; methodology, S.I. and J.S.; software, S.I.; validation, J.S., A.C., S.P. and M.G.; formal analysis, S.I.; investigation, S.I.; data curation, S.I. and D.Q.B.; writing—original draft preparation, S.I.; writing—review and editing, J.S., D.Q.B., A.C., S.P. and M.G.; supervision, J.S.; project administration, J.S.; funding acquisition, J.S. All authors have read and agreed to the published version of the manuscript.

Funding: This research was funded by PNRR H2IOSC (Humanities and Cultural Heritage Italian Open Science Cloud) Project (IR0000029), CUP_B63C2200073005, funded by Next Generation EU. The contents reflect only the authors' view, and the European Commission is not responsible for any use that may be made of the information it contains. The SHINE project funding (Strengthening the Italian Nodes of E-RIHS, Avviso 424/2018 dell'Azione II.1 PON R&I 2014–2020, DD n. 461 del 14-03-2019, PIR01_00016, CUP B27E19000030007) is acknowledged.

Data Availability Statement: The data presented in this study are available on request from the corresponding author and will be made available online at <https://hsg.ino.cnr.it/> (accessed on 26 May 2024).

Conflicts of Interest: The authors declare no conflicts of interest. The funders had no role in the design of the study; in the collection, analyses, or interpretation of data; in the writing of the manuscript; or in the decision to publish the results.

Appendix A

Table A1. Summary of the main Raman bands at 852 nm laser excitation (the most intense band is underlined) and their tentative assignment as from the literature.

Name	Band Wavenumber (cm^{-1}) and Relative Intensity at 852 nm of Laser Excitation	Raman Assignments	Figure
Cobalt blue [64]	204 410 <u>514</u> , 615 754	Complete transition of AO_4 $\delta_s \text{AO}_4$ $\nu_{as} \text{AO}_4$ $\nu_s \text{AO}_4$	Figure 4a
Prussian blue [65]	<u>275</u> , 538	Fe-CN-Fe deformation vibration and $\nu_s \text{Fe-C}$	Figure 4b
Antwerp blue	275, 533	* See Prussian blue	Figure 4c

Table A1. Cont.

Name	Band Wavenumber (cm ⁻¹) and Relative Intensity at 852 nm of Laser Excitation	Raman Assignments	Figure
Ultramarine blue [67]	258 375 548 1096	δS^{3-} - $\nu_s S^{3-}$ $3\nu_s S^{3-}$	Figure 4d
Azurite [68]	320, <u>404</u> 939 1095	Lattice mode $\delta O-H$ out-of-plane $\nu_s CO_3$	Figure 4e
Indigo [70]	674 756 1225 1360, <u>1571</u> , 1622 1470 1571	- - $\rho N-H$ $\nu_s C=C, C=O,$ and $N-H$ $\rho C-H$ $\nu_s C=C, C=O,$ and $N-H$	Figure 4f
Smalt [71]	195, 481, 620 <u>689</u>	The breathing vibration mode of the T-O-T substructure Si-O-Si vibration mode of SiO ₄	Figure 4g
Lapis lazuli [74]	548 <u>1306</u>	$\nu_s S^{3-}$ Luminescence band of minerals accompanying genuine lazurite	Figure 4h
Green earth [20]	200, <u>277</u> 393, 545	Internal vibrations of the MoO ₆ vibrational Modes of the SiO ₄	Figure 5a
Cobalt green [20]	340, 460, 520 <u>713</u>	- $\nu_s CoO_6$	Figure 5b
Chromium oxide [80]	297, 350, 528, 615 <u>554</u>	E _g A _{1g}	Figure 5c
Viridian [81]	<u>262</u> 487, 584	CrO ₂ $\alpha-CrOOH$	Figure 5d
Malachite [69]	219, 270, 350, <u>430</u> 816, 834 1095	Lattice mode $\delta_s CO_3$ $\nu_s CO_3$	Figure 5e
Massicot [45]	<u>290</u> , 385	-	Figure 6a
Lead-tin yellow [82]	<u>197</u> 275, 290, 455, 524	$\nu_s Pb-O$ -	Figure 6b
Naples yellow [83]	<u>290</u> , 318, 348, 440 510 613	Vibrational mode of Sb-O and PbO $\nu_s Sb-O$ -	Figure 6c
Chrome yellow [45]	339, 360, 379, 402 <u>841</u>	- $\nu_s Cr-O$	Figure 6d
Cadmium yellow [84,85]	<u>212</u> 298, 597	LA of ZnS crystal lattice LO+2E2 + overtones 2LO+2E2 of CdS crystal lattice	Figure 6e
Yellow ochre [86]	240, 480 300 <u>387</u> 549	- $\delta_s Fe-OH$ $\nu_s Fe-O-Fe/-OH$ $\nu_{as} Fe-OH$	Figure 6f

Table A1. Cont.

Name	Band Wavenumber (cm ⁻¹) and Relative Intensity at 852 nm of Laser Excitation	Raman Assignments	Figure
Raw sienna [86]	240, 480 300 390 550	- δ_s Fe-OH ν_s Fe-O-Fe/-OH ν_{as} Fe-OH	Figure 6g
Caput mortuum and umber [45]	222, 494 295,612 407	ν_s Fe-O δ_s Fe-O ν_s Fe-O-Fe/-OH	Figure 7a,b
Red bole [86]	225 296, 614 407	ν_s Fe-O Symmetric bending Fe-O ν_{as} Fe-O-Fe/-OH	Figure 7c
Cinnabar [87]	251, 284, 343	ν_s HgS	Figure 7d
Carmin naccarat [88]	471 1110 1252 1313 1358 1426 1491 1530	Skeletal vibrations δ (OH) + δ (CH) Gly δ (OH) + δ (CH) + δ ring Gly Gly δ CH(m) δ (OH) + δ (CH) -	Figure 7e
Alizarin crimson	238, 483, 655, 840, 903, 1020, 1047, 1164, 1190, 1223, 1292, 1328, 1358, 1480, 1522, 1574,1639	-	Figure 7f
Lead white [68,89]	329, 417 681, 1051 1365, 1484	- CCO ₃ ²⁻ ν_{as} CO ₃ ²⁻	Figure 8a
Selenite, gypsum [78]	316 413, 495 620, 674 1008 1133, 1476	T(H ₂ O, Ca) δ_s SO ₄ ²⁻ δ_{as} SO ₄ ²⁻ ν_s SO ₄ ²⁻ ν_{as} SO ₄ ²⁻	Figure 8b
Calcite [68]	285 714 1087 1437	Translatory oscillations of CO ₃ δ_{as} CO ₃ ²⁻ ν_a CO ₃ ²⁻ ν_{as} CO ₃ ²⁻	Figure 8c
Barite [90]	460 619, 644 989 1079, 1105, 1141, 1166	δ_s SO ₄ ²⁻ δ_{as} SO ₄ ²⁻ ν_s SO ₄ ²⁻ ν_{as} SO ₄ ²⁻	Figure 8d
Zinc oxide [91]	440, 336, 581 1156	- Boundary photons	Figure 8e
Ivory black [19]	1336 1603	C-C A _{1g} C-C in-plane stretching	Figure 8f

δ_s : symmetric bending; δ_{as} : asymmetric bending; ν_s : symmetric stretching; ν_{as} : asymmetric stretching; ρ : rocking; LO: longitudinal optic phonon; LA: longitudinal acoustic phonon; Gly: normal modes localized on glycosidic moiety; A_{1g}: A: symmetric species concerning the principal axis of symmetry, 1 (subscript): symmetric concerning a C₂ axis that is perpendicular to the principal axis, g (subscript): symmetric concerning a center of symmetry; E_{2g}: E: doubly degenerate, two-dimensional irreducible representation, g (subscript): symmetric concerning a center of symmetry; T: transitional model.

References

1. Vandenberghe, P. *Practical Raman Spectroscopy: An Introduction*; Wiley: Chichester, UK, 2013; ISBN 978-1-119-96190-1.
2. Odelli, E.; Rousaki, A.; Raneri, S.; Vandenberghe, P. Advantages and Pitfalls of the Use of Mobile Raman and XRF Systems Applied on Cultural Heritage Objects in Tuscany (Italy). *Eur. Phys. J. Plus* **2021**, *136*, 449. [CrossRef]
3. Bell Ian, M.; Clark Robin, J.K.; Peter, J. Gibbs Raman Spectroscopic Library of Natural and Synthetic Pigments (Pre-N 1850 AD). *Spectrochim. Acta Part A* **1997**, *53*, 2159–2179. [CrossRef]
4. Home | IRUG. Available online: <http://www.irug.org/> (accessed on 28 March 2024).
5. Cortea, I.M.; Anghelută, L.; Chiroșca, A.; Seritan, G. INFRA-ART Spectral Library: A New Open Access Infrastructure for Heritage Science. In *Lasers in the Conservation of Artworks XIII*; CRC Press: London, UK, 2023; pp. 37–47; ISBN 978-1-00-338687-2.
6. Lafuente, B.; Downs, R.T.; Yang, H.; Stone, N. 1. The Power of Databases: The RRUFF Project. In *Highlights in Mineralogical Crystallography*; Armbruster, T., Danisi, R.M., Eds.; De Gruyter: Berlin, Germany, 2015; pp. 1–30; ISBN 978-3-11-041704-3.
7. FT Raman Reference Spectra of Inorganics | The Infrared and Raman Discussion Group. Available online: <https://www.irdg.org/ijvs/library-of-spectra> (accessed on 28 March 2024).
8. SOPRANO. Available online: <https://soprano.kikirpa.be/> (accessed on 28 March 2024).
9. Caggiani, M.C.; Cosentino, A.; Mangone, A. Pigments Checker Version 3.0, a Handy Set for Conservation Scientists: A Free Online Raman Spectra Database. *Microchem. J.* **2016**, *129*, 123–132. [CrossRef]
10. Burgio, L.; Clark, R.J.H. Library of FT-Raman Spectra of Pigments, Minerals, Pigment Media and Varnishes, and Supplement to Existing Library of Raman Spectra of Pigments with Visible Excitation. *Spectrochim. Acta Part A Mol. Biomol. Spectrosc.* **2001**, *57*, 1491–1521. [CrossRef] [PubMed]
11. Lomax, S.Q. The IRUG Raman Spectral Web Database: Objectives, Progress and Plans. *E-Preserv. Sci.* **2013**, *10*, 38–41.
12. Buzgar, N.; Apopei, A.; Buzatu, A. Romanian Database of Raman Spectroscopy. 2009. Available online: <http://rdrs.uaic.ro/> (accessed on 28 March 2024).
13. Fremout, W.; Saverwyns, S. Identification of Synthetic Organic Pigments: The Role of a Comprehensive Digital Raman Spectral Library. *J. Raman Spectrosc.* **2012**, *43*, 1536–1544. [CrossRef]
14. Vandenberghe, P.; Moens, L.; Edwards, H.G.M.; Dams, R. Raman Spectroscopic Database of Azo Pigments and Application to Modern Art Studies. *J. Raman Spectrosc.* **2000**, *31*, 509–517. [CrossRef]
15. Bouchard, M.; Smith, D.C. Catalogue of 45 Reference Raman Spectra of Minerals Concerning Research in Art History or Archaeology, Especially on Corroded Metals and Coloured Glass. *Spectrochim. Acta Part A Mol. Biomol. Spectrosc.* **2003**, *59*, 2247–2266. [CrossRef] [PubMed]
16. Scherrer, N.C.; Stefan, Z.; Francoise, D.; Annette, F.; Renate, K. Synthetic Organic Pigments of the 20th and 21st Century Relevant to Artist's Paints: Raman Spectra Reference Collection. *Spectrochim. Acta Part A Mol. Biomol. Spectrosc.* **2009**, *73*, 505–524. [CrossRef]
17. Martina, I.; Wiesinger, R.; Jembrith-Simburger, D.; Schreiner, M. Micro-Raman Characterisation of Silver Corrosion Products: Instrumental Set up and Reference Database. *E-Preserv. Sci.* **2012**, *9*, 1–8.
18. Pozzi, F.; Lombardi, J.R.; Leona, M. Winsor & Newton Original Handbooks: A Surface-Enhanced Raman Scattering (SERS) and Raman Spectral Database of Dyes from Modern Watercolor Pigments. *Herit. Sci.* **2013**, *1*, 23.
19. Coccato, A.; Jehlička, J.; Moens, L.; Vandenberghe, P. Raman Spectroscopy for the Investigation of Carbon-based Black Pigments. *J. Raman Spectrosc.* **2015**, *46*, 1003–1015. [CrossRef]
20. Coccato, A.; Bersani, D.; Coudray, A.; Sanyova, J.; Moens, L.; Vandenberghe, P. Raman Spectroscopy of Green Minerals and Reaction Products with an Application in Cultural Heritage Research. *J. Raman Spectrosc.* **2016**, *47*, 1429–1443. [CrossRef]
21. Marucci, G.; Beeby, A.; Parker, A.W.; Nicholson, C.E. Raman Spectroscopic Library of Medieval Pigments Collected with Five Different Wavelengths for Investigation of Illuminated Manuscripts. *Anal. Methods* **2018**, *10*, 1219–1236. [CrossRef]
22. Culka, A.; Jehlička, J. Identification of Gemstones Using Portable Sequentially Shifted Excitation Raman Spectrometer and RRUFF Online Database: A Proof of Concept Study. *Eur. Phys. J. Plus* **2019**, *134*, 130. [CrossRef]
23. Burrafato, G.; Calabrese, M.; Cosentino, A.; Gueli, A.M.; Troja, S.O.; Zuccarello, A. ColoRaman Project: Raman and Fluorescence Spectroscopy of Oil, Tempera and Fresco Paint Pigments. *J. Raman Spectrosc.* **2004**, *35*, 879–886. [CrossRef]
24. Castro, K.; Pérez-Alonso, M.; Rodríguez-Laso, M.D.; Fernández, L.A.; Madariaga, J.M. On-Line FT-Raman and Dispersive Raman Spectra Database of Artists' Materials (e-VISART Database). *Anal. Bioanal. Chem.* **2005**, *382*, 248–258. [CrossRef]
25. Sessa, C.; Steuer, C.; Quintero Balbas, D.; Sciutto, G.; Prati, S.; Stege, H. Analytical Studies on Commercial Artists' Colour Charts from Das Deutsche Farbenbuch (1925)—Identification of Synthetic and Natural Organic Colourants by Raman Microscopy, Surface-Enhanced Raman Spectroscopy and Metal Underlayer ATR-FTIR Spectroscopy. *Herit. Sci.* **2022**, *10*, 109. [CrossRef]
26. Thorley, F.C.; Baldwin, K.J.; Lee, D.C.; Batchelder, D.N. Dependence of the Raman Spectra of Drug Substances upon Laser Excitation Wavelength. *J. Raman Spectrosc.* **2006**, *37*, 335–341. [CrossRef]
27. Ferraro, J.R.; Nakamoto, K.; Brown, C.W. *Introductory Raman Spectroscopy*, 2nd ed.; Academic Press: Amsterdam, The Netherlands; Boston, MA, USA, 2003; ISBN 978-0-12-254105-6.
28. Conti, C.; Botteon, A.; Bertasa, M.; Colombo, C.; Realini, M.; Sali, D. Portable Sequentially Shifted Excitation Raman Spectroscopy as an Innovative Tool for in Situ Chemical Interrogation of Painted Surfaces. *Analyst* **2016**, *141*, 4599–4607. [CrossRef]
29. Jehlička, J.; Culka, A. Critical Evaluation of Portable Raman Spectrometers: From Rock Outcrops and Planetary Analogs to Cultural Heritage—A Review. *Anal. Chim. Acta* **2022**, *1209*, 339027. [CrossRef]

30. Vagnini, M.; Gabrieli, F.; Daveri, A.; Sali, D. Handheld New Technology Raman and Portable FT-IR Spectrometers as Complementary Tools for the in Situ Identification of Organic Materials in Modern Art. *Spectrochim. Acta Part A Mol. Biomol. Spectrosc.* **2017**, *176*, 174–182. [[CrossRef](#)] [[PubMed](#)]
31. Daveri, A.; Paziani, S.; Marmion, M.; Harju, H.; Vidman, A.; Azzarelli, M.; Vagnini, M. New Perspectives in the Non-Invasive, in Situ Identification of Painting Materials: The Advanced MWIR Hyperspectral Imaging. *TrAC Trends Anal. Chem.* **2018**, *98*, 143–148. [[CrossRef](#)]
32. Pozzi, F.; Basso, E.; Rizzo, A.; Cesaratto, A.; Tague, T.J. Evaluation and Optimization of the Potential of a Handheld Raman Spectrometer: In Situ, Noninvasive Materials Characterization in Artworks. *J. Raman Spectrosc.* **2019**, *50*, 861–872. [[CrossRef](#)]
33. Mollica Nardo, V.; Renda, V.; Bonanno, S.; Parrotta, F.; Anastasio, G.; Caponetti, E.; Saladino, M.L.; Vasi, C.S.; Ponterio, R.C. Non-Invasive Investigation of Pigments of Wall Painting in S. Maria Delle Palate Di Tusa (Messina, Italy). *Heritage* **2019**, *2*, 2398–2407. [[CrossRef](#)]
34. Alberghina, M.F.; Germinario, C.; Bartolozzi, G.; Bracci, S.; Grifa, C.; Izzo, F.; La Russa, M.F.; Magrini, D.; Massa, E.; Mercurio, M.; et al. Non-Invasive Characterization of the Pigment's Palette Used on the Painted Tomb Slabs at Paestum Archaeological Site. *IOP Conf. Ser. Mater. Sci. Eng.* **2020**, *949*, 012002. [[CrossRef](#)]
35. Dal Fovo, A.; Striova, J.; Pampaloni, E.; Fedele, A.; Morita, M.M.; Amaya, D.; Grazzi, F.; Cimò, M.; Cirrincione, C.; Fontana, R. Rubens' Painting as Inspiration of a Later Tapestry: Non-Invasive Analyses Provide Insight into Artworks' History. *Microchem. J.* **2020**, *153*, 104472. [[CrossRef](#)]
36. Giuffrida, D.; Mollica Nardo, V.; Neri, D.; Cucinotta, G.; Calabrò, I.V.; Pace, L.; Ponterio, R.C. A Multi-Analytical Study for the Enhancement and Accessibility of Archaeological Heritage: The Churches of San Nicola and San Basilio in Motta Sant'Agata (RC, Italy). *Remote Sens.* **2021**, *13*, 3738. [[CrossRef](#)]
37. Sharma, A.; Singh, M.R. Execution Technique and Pigment Characteristics of Decorative Wall from 17th CE Chatta Chowk, Red Fort Complex, New Delhi. *Period. Di Mineral.* **2020**, *90*, 43–56. [[CrossRef](#)]
38. Amadori, M.L.; Mengacci, V.; Vagnini, M.; Casoli, A.; Holakooei, P.; Eftekhari, N.; Lin, K.; Maekawa, Y.; Germinario, G. Organic Matter and Pigments in the Wall Paintings of Me-Taw-Ya Temple in Bagan Valley, Myanmar. *Appl. Sci.* **2021**, *11*, 11441. [[CrossRef](#)]
39. Amadori, M.L.; Vagnini, M.; Vivani, R.; Anselmi, C.; Chaverdi, A.A.; Callieri, P.; Matin, E.; Mengacci, V. Advances in Characterization of Colourful Residues Unearthed in Persepolis West Craft Zone Using Microscopic and Spectroscopic Techniques. *Microchem. J.* **2021**, *167*, 106304. [[CrossRef](#)]
40. Invernizzi, C.; Fiocco, G.; Iwanicka, M.; Targowski, P.; Piccirillo, A.; Vagnini, M.; Licchelli, M.; Malagodi, M.; Bersani, D. Surface and Interface Treatments on Wooden Artefacts: Potentialities and Limits of a Non-Invasive Multi-Technique Study. *Coatings* **2020**, *11*, 29. [[CrossRef](#)]
41. Vagnini, M.; Anselmi, C.; Azzarelli, M.; Sgamellotti, A. Things Always Come in Three: Non-Invasive Investigations of Alexander and Roxane's Wedding Room in Villa Farnesina. *Heritage* **2021**, *4*, 2792–2809. [[CrossRef](#)]
42. Gargano, M.; Longoni, M.; Pesce, V.; Palandri, M.C.; Canepari, A.; Ludwig, N.; Bruni, S. From Materials to Technique: A Complete Non-Invasive Investigation of a Group of Six Ukiyo-E Japanese Woodblock Prints of the Oriental Art Museum E. Chiossone (Genoa, Italy). *Sensors* **2022**, *22*, 8772. [[CrossRef](#)] [[PubMed](#)]
43. Longoni, M.; Beccaria, C.; Bonizzoni, L.; Bruni, S. A Silver Monochrome "Concetto Spaziale" by Lucio Fontana: A Spectroscopic Non- and Micro-Invasive Investigation of Materials. *Molecules* **2022**, *27*, 4442. [[CrossRef](#)]
44. Festa, G.; Scatigno, C.; Armetta, F.; Saladino, M.L.; Ciaramitaro, V.; Nardo, V.M.; Ponterio, R.C. Chemometric Tools to Point Out Benchmarks and Chromophores in Pigments through Spectroscopic Data Analyses. *Molecules* **2021**, *27*, 163. [[CrossRef](#)] [[PubMed](#)]
45. Innocenti, S.; Quintero Balbas, D.; Pezzati, L.; Fontana, R.; Striova, J. Portable Sequentially Shifted Excitation Raman Spectroscopy to Examine Historic Powders Enclosed in Glass Vials. *Sensors* **2022**, *22*, 3560. [[CrossRef](#)] [[PubMed](#)]
46. Ciaramitaro, V.; Armetta, F.; Mollica Nardo, V.; Ponterio, R.C.; Saladino, M.L. Portable Spectroscopic Techniques for the Non-Invasive Identification of Two Historical Yellow Pigments: Applications and Practical Challenges. *J. Phys. Conf. Ser.* **2022**, *2204*, 012056. [[CrossRef](#)]
47. Beck, M.E.; MacDonald, B.L.; Ferguson, J.R.; Adair, M.J. Red Pigment in the Central Plains: A Pawnee Case at Kitkahahki Town. *Plains Anthropol.* **2022**, *67*, 405–430. [[CrossRef](#)]
48. Giuffrida, D.; Bonanno, S.; Parrotta, F.; Mollica Nardo, V.; Anastasio, G.; Saladino, M.L.; Armetta, F.; Ponterio, R.C. The Church of S. Maria Delle Palate in Tusa (Messina, Italy): Digitization and Diagnostics for a New Model of Enjoyment. *Remote Sens.* **2022**, *14*, 1490. [[CrossRef](#)]
49. Raicu, T.; Zollo, F.; Falchi, L.; Barisoni, E.; Piccolo, M.; Izzo, F.C. Preliminary Identification of Mixtures of Pigments Using the paletteR Package in R—The Case of Six Paintings by Andreina Rosa (1924–2019) from the International Gallery of Modern Art Ca' Pesaro, Venice. *Heritage* **2023**, *6*, 524–547. [[CrossRef](#)]
50. Vavřík, D.; Antušková, V.; Chlumská, Š.; Kumpová, I.; Šefců, R.; Vopálenský, M. Non-Destructive Exploration of Late Gothic Panel Painting Using X-Ray Tomography and Flattening of the Reconstructed Data. *Eur. Phys. J. Plus* **2023**, *138*, 618. [[CrossRef](#)]
51. Volpi, F.; Vagnini, M.; Vivani, R.; Malagodi, M.; Fiocco, G. Non-Invasive Identification of Red and Yellow Oxide and Sulfide Pigments in Wall-Paintings with Portable ER-FTIR Spectroscopy. *J. Cult. Herit.* **2023**, *63*, 158–168. [[CrossRef](#)]
52. Morales Toledo, E.G.; Raicu, T.; Falchi, L.; Barisoni, E.; Piccolo, M.; Izzo, F.C. Critical Analysis of the Materials Used by the Venetian Artist Guido Cadorin (1892–1976) during the Mid-20th Century, Using a Multi-Analytical Approach. *Heritage* **2023**, *6*, 600–627. [[CrossRef](#)]

53. Bottura-Scardina, S.; Vandenabeele, P.; Miguel, C.; Candeias, A. Comparative Assessment of Two Portable Raman Spectrometers for the Characterisation of Historical Natural Dye Lakes. *J. Raman Spectrosc.* **2023**, *54*, 1303–1313. [[CrossRef](#)]
54. Culka, A.; Hyršl, J.; Jehlička, J. Gem and Mineral Identification Using GL Gem Raman and Comparison with Other Portable Instruments. *Appl. Phys. A* **2016**, *122*, 959. [[CrossRef](#)]
55. Pozzi, F.; Basso, E.; Snyder, R. Color, Collation, and Curious Creatures: A Technical Study of 15th-Century Block Books at The Morgan Library & Museum. *Eur. Phys. J. Plus* **2021**, *136*, 414. [[CrossRef](#)]
56. Oubelkacem, Y.; Lamhasni, T.; El Bakkali, A.; Lyazidi, S.A.; Haddad, M.; Ben-Ncer, A. Parchments and Coloring Materials in Two IXth Century Manuscripts: On-Site Non-Invasive Multi-Techniques Investigation. *Spectrochim. Acta Part A Mol. Biomol. Spectrosc.* **2021**, *247*, 119093. [[CrossRef](#)] [[PubMed](#)]
57. Rousaki, A.; Costa, M.; Saelens, D.; Lycke, S.; Sánchez, A.; Tuñón, J.; Ceprián, B.; Amate, P.; Montejo, M.; Mirão, J.; et al. A Comparative Mobile Raman Study for the on Field Analysis of the *Mosaico de Los Amores* of the Cástulo Archaeological Site (Linares, Spain). *J. Raman Spectrosc.* **2020**, *51*, 1913–1923. [[CrossRef](#)]
58. Porcu, D.; Innocenti, S.; Galeotti, M.; Striova, J.; Dei, L.; Carretti, E.; Fontana, R. Spectroscopic and Morphologic Investigation of Bronze Disease: Performance Evaluation of Portable Devices. *Heritage* **2022**, *5*, 3548–3561. [[CrossRef](#)]
59. Porcaro, M.; Lins, S.; Depalmas, A.; Anzalone, R.M.; Iannaccone, R.; Brunetti, A. Characterization of a Unique Nuragic Bronze Navicella with a Combination of X-Ray Fluorescence Spectrometry and Monte Carlo Simulation. *Materials* **2023**, *16*, 7345. [[CrossRef](#)] [[PubMed](#)]
60. Armetta, F.; Ponterio, R.C.; Pibiri, I.; Saladino, M.L. New Insight on Archaeological Metal Finds, Nails and Lead Sheathings of the Punic Ship from Battle of the Egadi Islands. *Molecules* **2023**, *28*, 1968. [[CrossRef](#)] [[PubMed](#)]
61. Feller, R.L. *Artists' Pigments: A Handbook of Their History and Characteristics*; National Gallery of Art: Washington, DC, USA, 1986; ISBN 978-0-89468-086-1.
62. Roy, A. *Artists' Pigments: A Handbook of Their History and Characteristics*; National Gallery of Art: Washington, DC, USA, 1993; ISBN 978-1-904982-75-3.
63. Fitzhugh, E.W. *Artists' Pigments: A Handbook of Their History and Characteristics*; National Gallery of Art: Washington, DC, USA, 1997; ISBN 978-1-904982-76-0.
64. D'Ippolito, V.; Andreozzi, G.B.; Bersani, D.; Lottici, P.P. Raman Fingerprint of Chromate, Aluminate and Ferrite Spinels. *J. Raman Spectrosc.* **2015**, *46*, 1255–1264. [[CrossRef](#)]
65. Moretti, G.; Gervais, C. Raman Spectroscopy of the Photosensitive Pigment Prussian Blue. *J. Raman Spectrosc.* **2018**, *49*, 1198–1204. [[CrossRef](#)]
66. Antwerp Blue—CAMEO. Available online: https://cameo.mfa.org/wiki/Antwerp_blue (accessed on 28 March 2024).
67. Osticioli, I.; Mendes, N.F.C.; Nevin, A.; Gil, F.P.S.C.; Becucci, M.; Castellucci, E. Analysis of Natural and Artificial Ultramarine Blue Pigments Using Laser Induced Breakdown and Pulsed Raman Spectroscopy, Statistical Analysis and Light Microscopy. *Spectrochim. Acta Part A Mol. Biomol. Spectrosc.* **2009**, *73*, 525–531. [[CrossRef](#)] [[PubMed](#)]
68. Buzgar, N.; Apopei, A. The Raman Study of Certain Carbonates. *Geol. Tomul L* **2009**, *2*, 97–112.
69. Frost, R.L.; Martens, W.N.; Rintoul, L.; Mahmutagic, E.; Klopogge, J.T. Raman Spectroscopic Study of Azurite and Malachite at 298 and 77 K. *J. Raman Spectrosc.* **2002**, *33*, 252–259. [[CrossRef](#)]
70. Baran, A.; Fiedler, A.; Schulz, H.; Baranska, M. In Situ Raman and IR Spectroscopic Analysis of Indigo Dye. *Anal. Methods* **2010**, *2*, 1372. [[CrossRef](#)]
71. Sharma, S.K.; Mammoni, J.F.; Nicol, M.F. Raman Investigation of Ring Configurations in Vitreous Silica. *Nature* **1981**, *292*, 140–141. [[CrossRef](#)]
72. Mihailova, B.; Zotov, N.; Marinov, M.; Nikolov, J.; Konstantinov, L. Vibrational Spectra of Rings in Silicate Glasses. *J. Non-Cryst. Solids* **1994**, *168*, 265–274. [[CrossRef](#)]
73. Schmidt, C.M.; Walton, M.S.; Trentelman, K. Characterization of *Lapis Lazuli* Pigments Using a Multitechnique Analytical Approach: Implications for Identification and Geological Provenancing. *Anal. Chem.* **2009**, *81*, 8513–8518. [[CrossRef](#)] [[PubMed](#)]
74. González-Cabrera, M.; Arjonilla, P.; Domínguez-Vidal, A.; Ayora-Cañada, M.J. Natural or Synthetic? Simultaneous Raman/Luminescence Hyperspectral Microimaging for the Fast Distinction of Ultramarine Pigments. *Dye. Pigment.* **2020**, *178*, 108349. [[CrossRef](#)]
75. Spoto, S.E.; Somma, R.; Paladini, G.; Caridi, F.; Interdonato, M.; Majolino, D.; Venturi, V. From Lapis Lazuli to Synthetic Ultramarines: A μ -Raman Spectroscopy Investigation on the History and Development of “the Most Perfect” Color. In Proceedings of the 2022 IMEKO TC4 International Conference on Metrology for Archaeology and Cultural Heritage, University of Calabria, Calabria, Italy, 19–21 October 2022.
76. Saleh, M. Validation with Raman Spectroscopy of Lapis Lazuli Provenance Study. *Nuovo C. Soc. Ital. Fis. C Geophys. Space Phys.* **2021**, *44*, 24. [[CrossRef](#)]
77. Colomban, P. Lapis Lazuli as Unexpected Blue Pigment in Iranian Lajvardina Ceramics. *J. Raman Spectrosc.* **2003**, *34*, 420–423. [[CrossRef](#)]
78. Sarma, L.P.; Prasad, P.S.R.; Ravikumar, N. Raman Spectroscopic Study of Phase Transitions in Natural Gypsum. *J. Raman Spectrosc.* **1998**, *29*, 851–856. [[CrossRef](#)]
79. Ospitali, F.; Bersani, D.; Di Lonardo, G.; Lottici, P.P. ‘Green Earths’: Vibrational and Elemental Characterization of Glauconites, Celadonites and Historical Pigments. *J. Raman Spectrosc.* **2008**, *39*, 1066–1073. [[CrossRef](#)]

80. Vuurman, M.A.; Stufkens, D.J.; Oskam, A.; Moulijn, J.A.; Kapteijn, F. Raman Spectra of Chromium Oxide Species in CrO₃/Al₂O₃ Catalysts. *J. Mol. Catal.* **1990**, *60*, 83–98. [[CrossRef](#)]
81. Maslar, J.E.; Hurst, W.S.; Bowers, W.J.; Hendricks, J.H.; Aquino, M.I.; Levin, I. In Situ Raman Spectroscopic Investigation of Chromium Surfaces under Hydrothermal Conditions. *Appl. Surf. Sci.* **2001**, *180*, 102–118. [[CrossRef](#)]
82. Šefců, R.; Chlumská, Š.; Hostašová, A. An Investigation of the Lead Tin Yellows Type I and II and Their Use in Bohemian Panel Paintings from the Gothic Period. *Herit. Sci.* **2015**, *3*, 16. [[CrossRef](#)]
83. Rosi, F.; Manuali, V.; Grygar, T.; Bezdicka, P.; Brunetti, B.G.; Sgamellotti, A.; Burgio, L.; Seccaroni, C.; Miliiani, C. Raman Scattering Features of Lead Pyroantimonate Compounds: Implication for the Non-invasive Identification of Yellow Pigments on Ancient Ceramics. Part II. In Situ Characterisation of Renaissance Plates by Portable micro-Raman and XRF Studies. *J. Raman Spectrosc.* **2011**, *42*, 407–414. [[CrossRef](#)]
84. Kumar, P.; Saxena, N.; Chandra, R.; Gupta, V.; Agarwal, A.; Kanjilal, D. Nanotwinning and Structural Phase Transition in CdS Quantum Dots. *Nanoscale Res. Lett.* **2012**, *7*, 584. [[CrossRef](#)] [[PubMed](#)]
85. Xiong, Q.; Wang, J.; Reese, O.; Lew Yan Voon, L.C.; Eklund, P.C. Raman Scattering from Surface Phonons in Rectangular Cross-Sectional w-ZnS Nanowires. *Nano Lett.* **2004**, *4*, 1991–1996. [[CrossRef](#)]
86. Legodi, M.; Dewaal, D. The Preparation of Magnetite, Goethite, Hematite and Maghemite of Pigment Quality from Mill Scale Iron Waste. *Dye. Pigment.* **2007**, *74*, 161–168. [[CrossRef](#)]
87. Frost, R.L.; Martens, W.N.; Kloprogge, J.T. Raman Spectroscopic Study of Cinnabar (HgS), Realgar (As₄S₄), and Orpiment (As₂S₃) at 298 and 77K. *Neues Jahrb. Fuer Mineral. Monatshefte* **2002**, *10*, 469–480. [[CrossRef](#)]
88. Innocenti, S.; Ricci, M.; Lanterna, G.; Fontana, R.; Striova, J.; Becucci, M. Direct Microextraction for Red Lakes Detection in Painting Layers by Raman Spectroscopy. *Eur. Phys. J. Plus* **2021**, *136*, 1081. [[CrossRef](#)]
89. Tomić, Z.; Makreski, P.; Gajić, B. Identification and Spectra–Structure Determination of Soil Minerals: Raman Study Supported by IR Spectroscopy and X-ray Powder Diffraction. *J. Raman Spectrosc.* **2010**, *41*, 582–586. [[CrossRef](#)]
90. Buzgar, N.; Buzatu, A.; Sanislav, I.V. The Raman Study on Certain Sulfates. *Sci. Ann. Univ. Al. I. Cuza Iași* **2009**, *55*, 5–23.
91. Du, Y.; Zhang, M.-S.; Hong, J.; Shen, Y.; Chen, Q.; Yin, Z. Structural and Optical Properties of Nanophase Zinc Oxide. *Appl. Phys. A Mater. Sci. Process.* **2003**, *76*, 171–176. [[CrossRef](#)]

Disclaimer/Publisher’s Note: The statements, opinions and data contained in all publications are solely those of the individual author(s) and contributor(s) and not of MDPI and/or the editor(s). MDPI and/or the editor(s) disclaim responsibility for any injury to people or property resulting from any ideas, methods, instructions or products referred to in the content.